# Strategies for accessing photosensitizers with extreme redox potentials •

Cite as: Chem. Phys. Rev. **3**, 021302 (2022); https://doi.org/10.1063/5.0084554 Submitted: 07 January 2022 • Accepted: 18 April 2022 • Published Online: 03 May 2022

Dooyoung Kim and Thomas S. Teets

#### **COLLECTIONS**

F This paper was selected as Featured







#### ARTICLES YOU MAY BE INTERESTED IN

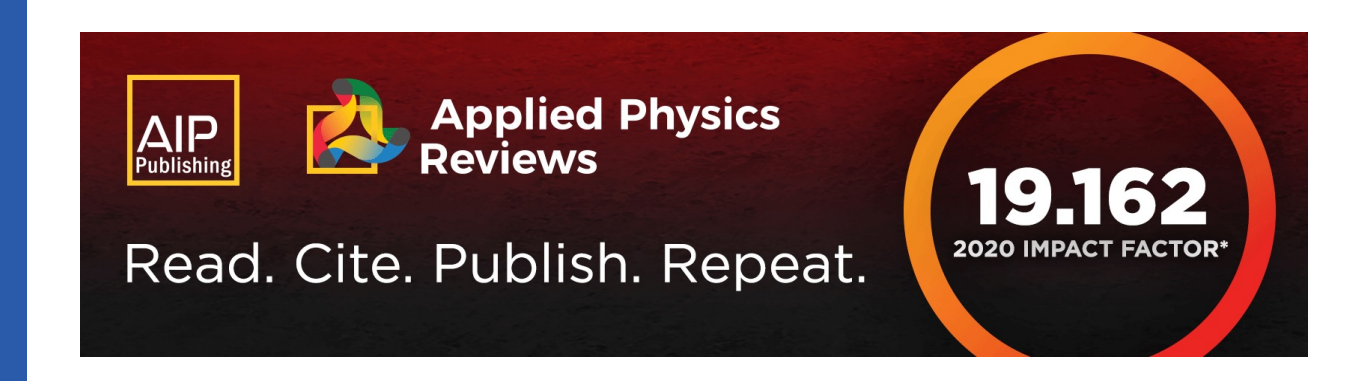
The fluorescence quantum yield parameter in Förster resonance energy transfer (FRET)—Meaning, misperception, and molecular design

Chemical Physics Reviews 2, 011302 (2021); https://doi.org/10.1063/5.0041132

Machine learning on neutron and x-ray scattering and spectroscopies Chemical Physics Reviews 2, 031301 (2021); https://doi.org/10.1063/5.0049111

Molecular library of OLED host materials—Evaluating the multiscale simulation workflow Chemical Physics Reviews 2, 031304 (2021); https://doi.org/10.1063/5.0049513







# Strategies for accessing photosensitizers with extreme redox potentials (1)

Cite as: Chem. Phys. Rev. **3**, 021302 (2022); doi: 10.1063/5.0084554 Submitted: 7 January 2022 · Accepted: 18 April 2022 · Published Online: 3 May 2022







Dooyoung Kim (b) and Thomas S. Teets<sup>a)</sup> (b)

#### **AFFILIATIONS**

Department of Chemistry, University of Houston, 3585 Cullen Boulevard Room 112, Houston, Texas 77204-5003, USA

a) Author to whom correspondence should be addressed: tteets@uh.edu

#### **ABSTRACT**

Photoredox catalysis has been prominent in many applications, including solar fuels, organic synthesis, and polymer chemistry. Photocatalytic activity directly depends on the photophysical and electrochemical properties of photocatalysts in both the ground state and excited state. Controlling those properties, therefore, is imperative to achieve the desired photocatalytic activity. Redox potential is one important factor that impacts both the thermodynamic and kinetic aspects of key elementary steps in photoredox catalysis. In many challenging reactions in organic synthesis, high redox potentials of the substrates hamper the reaction, leading to slow conversion. Thus, the development of photocatalysts with extreme redox potentials, accompanied by potent reducing or oxidizing power, is required to execute high-yielding thermodynamically demanding reactions. In this review, we will introduce strategies for accessing extreme redox potentials in photocatalytic transformations. These include molecular design strategies for preparing photosensitizers that are exceptionally strong ground-state or excited-state reductants or oxidants, highlighting both organic and metal-based photosensitizers. We also outline methodological approaches for accessing extreme redox potentials, using two-photon activation, or combined electrochemical/photochemical strategies to generate potent redox reagents from precursors that have milder potentials.

Published under an exclusive license by AIP Publishing. https://doi.org/10.1063/5.0084554

#### **TABLE OF CONTENTS**

I. INTRODUCTION	1
II. KEY FEATURES OF PHOTOSENSITIZERS	2
A. Photosensitization process	2
1. Photoinduced electron transfer	2
2. Investigating mechanisms	3
B. Photophysical and electrochemical properties	4
1. Excited-state energy	5
2. Ground- and excited-state redox potentials	5
3. Excited-state redox potential	5
III. STRATEGIES FOR HIGHLY REDUCING	
AND OXIDIZING PHOTOSENSITIZERS	5
A. Molecular design approaches	5
1. Acridinium chromophores	6
2. Cyanoarenes	7
3. Phenazine, phenoxazine, and phenothiazine	9
4. Ru(II) and Ir(III) complexes	10
5. Other metal complexes	12
	15
B. Two-photon activation	13
C. Combined photo- and electro-chemical	21
activations	21
IV. CONCLUSION	26

#### I. INTRODUCTION

Molecular photosensitizers (PSs), often referred to as photocatalysts in catalytic applications, are the organic molecules or transition metal coordination complexes that absorb UV to visible light and convert it to chemical potential, participating in energy or electron transfer (ET) processes after excitation. Earlier applications of photosensitizers were focused on areas related to solar energy capture and conversion, such as solar fuels<sup>1–3</sup> or photovoltaics.<sup>4–6</sup> Many pioneering works have recently demonstrated the applicability of photosensitizers in organic synthesis methodology, carrying out challenging organic reactions under mild conditions.<sup>7–13</sup> Historically, the common molecular photosensitizers used in photocatalysis are transition metal coordination complexes, often of ruthenium(II) or iridium(III), which can serve as efficient photosensitizers for a variety of applications.  $^{11,14,15}$  Metal-free organic chromophores also have drawn attention as good alternatives to transition metal-based photosensitizers, due to their relatively low cost and low toxicity. 13,1

The continued interest in this fast-emerging area motivates researchers to develop effective photosensitizers capable of promoting efficient photocatalytic reactions. There are many factors that determine the photocatalytic performance of photosensitizers, such as molar absorptivity, maximum absorption wavelength, emission

wavelength, excited-state energy, lifetime in the excited-state, quantum yield, and electrochemical properties including ground- or excited-state redox potentials. Of those factors, in many cases the photocatalytic performance is strongly correlated with the redox properties of the photosensitizer in both the ground and excited state, which has both kinetic and thermodynamic implications on the reaction. From a thermodynamic standpoint, more extreme oxidizing or reducing photosensitizer redox potentials allow challenging, redox-inert substrates to be activated. From a kinetic standpoint, the Marcus relationship (see below) stipulates that in many cases increasing the driving force of electron transfer increases the rate. Accordingly, photosensitizers with extreme redox potentials are essential to carry out thermodynamically challenging reactions with appreciable rates.

In this review, we will focus on strategies for accessing photosensitizers with extreme redox potentials, suitable for promoting thermodynamically challenging redox transformations. Acknowledging that there is no objective definition for "extreme redox potentials," most of the examples highlighted involve excited-state potentials more negative than -1.6 V vs saturated calomel electrode (SCE) for photoreductants, or excited-state potentials more positive than +0.8 V vs SCE for photooxidants (these potentials will be clearly defined in Sec. II B). The former value represents the approximate excited-state potential of iridium photosensitizers, which for many years were the strongest photoreductants commonly employed, and also is the starting point for the ground-state reduction potentials of unactivated organohalide substrates, which have presented a particular challenge in photoredox methodology. The latter represents the excited-state potential of common ruthenium polypyridyl photosensitizers, a versatile class of photooxidants. Regardless of the precise cutoffs for redox potentials, we emphasize literature examples that specifically describe strategies to increase the redox capabilities of common photosensitizer classes. This article is not designed to be comprehensive, but rather aims to teach the reader about the variety of strategies that have been discovered for accessing strongly reducing or oxidizing photosensitizers. The review starts with a general outline of photosensitization processes and summarizes key features that affect the photocatalytic properties of photosensitizers. Since this background has already been described in detail in some of our previous papers, 20-22 we will briefly introduce some of those features that are most relevant to the present review. The strategies described for accessing potent photosensitizers with strong and extreme redox potentials are divided into three categories. The largest section deals with molecular design strategies for accessing potent photosensitizers, highlighting both organic and metal-based photosensitizer classes. The other two sections highlight methodological approaches for challenging photoinduced redox transformations. These strategies use additional energy input in the form of two photons or electrochemical driving force to access potent excited-state redox potentials, from precursors that would not be particularly strong oxidants or reductants under conventional one-photon activation.

#### II. KEY FEATURES OF PHOTOSENSITIZERS

#### A. Photosensitization process

## 1. Photoinduced electron transfer

During the simplest and most general electron transfer process, one electron transfers from an electron donor (D) to an electron acceptor (A) and this process can be depicted as follows:

$$D + A \xrightarrow{k_{ET}} D^+ + A^-. \tag{1}$$

The kinetics of this electron transfer mechanism in the ground state can be described by Marcus theory, numerically represented as follows:<sup>23–25</sup>

$$k_{ET} = \frac{k_B T}{h} \exp\left[-\frac{(\lambda + \Delta G_0)^2}{4\lambda k_B T}\right]. \tag{2}$$

In Eq. (2),  $k_{\rm B}$  is the Boltzmann constant, T is the absolute temperature, h is Plank's constant,  $\lambda$  is the reorganization energy, and  $\Delta G_0$  is the driving force of the electron transfer reaction, which can be determined by the redox potential difference between the electron donor (D) and acceptor (A).

The Rehm–Weller equation [Eq. (3)] is another relevant empirical relationship, providing an estimate of the second-order rate constant  $(k_q)$  for an intermolecular photoinduced electron transfer process<sup>26–31</sup>

$$k_{q} = \frac{k_{d}}{1 + \frac{k_{d}}{K_{d}Z} \left[ \exp\left(\frac{\Delta G^{\ddagger}}{RT}\right) + \exp\left(\frac{\Delta G_{0}}{RT}\right) \right]}.$$
 (3)

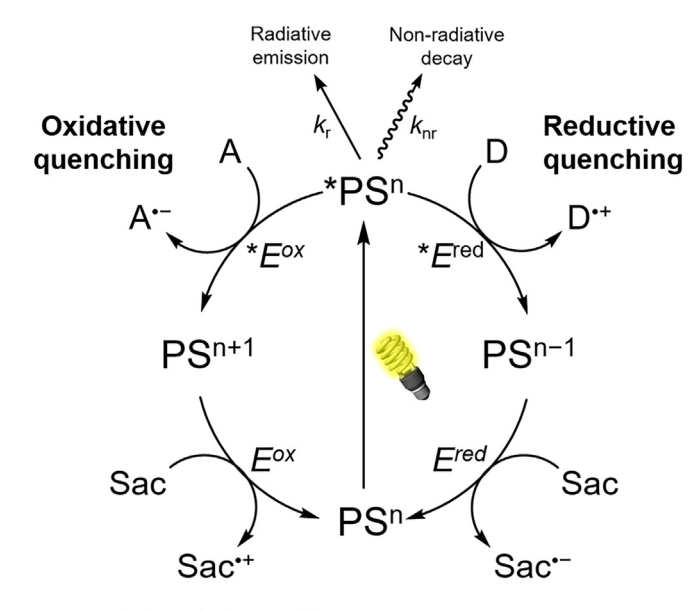
 $\Delta G_0$  is the Gibbs energy of photoinduced electron transfer;  $k_{\rm d}$  and  $K_{\rm d}$  are the forward rate constant and equilibrium constant, respectively, for the formation of the encounter complex; Z is the universal collision frequency factor; R is the gas constant; T is the temperature; and  $\Delta G^{\ddagger}$  is the activation Gibbs energy of the forward electron transfer reaction. Both of these relationships involve a driving force term, which in photocatalytic systems or more generally in photoinduced redox chemistry involves electron transfer between the excited state of the photosensitizer and an electron donor or acceptor. Therefore, photosensitizer's excited-state energy should be considered as well when estimating driving force

$$\Delta G_0 = E(PS^+/PS) - (E(A/A^-) + E(PS^*)) - w,$$
 (4a)

$$\Delta G_0 = (E(PS/PS^-) + E(PS^*)) - E(D^+/D) - w.$$
 (4b)

E represents the relevant redox potentials of the photosensitizer (PS), electron donor (D), and electron acceptor (A);  $E(PS^*)$  is the excited-state energy of PS; and w is an electrostatic work term. The redox potential and excited-state energy terms in Eqs. (4a) and (4b) will be defined more clearly in Sec. II B. Note that Eqs. (4a) and (4b) or closely related variants are sometimes also referred to as the Rehm–Weller equation, although according to IUPAC that notation is incorrect and only Eq. (3) should be described as the Rehm–Weller equation.  $^{32}$ 

As illustrated in Fig. 1, there are two major pathways for photoin-duced electron transfer: oxidative quenching and reductive quenching. Upon absorption of photon energy, the excited-state photosensitizer (\*PS") is produced, where n is the charge of the ground-state species. During oxidative quenching, \*PS" donates one electron to an acceptor (A) and is oxidized in the process. In this case, the PS is functioning as a photoreductant, and Eq. (4a) can be applied to this situation. In the reductive quenching pathway, electron transfer from the donor (D) to \*PS" occurs, generating reduced PS" $^{-1}$ , with PS functioning as a photooxidant in this case. Equation (4b) can be applied to reductive



PS = photosensitizer A = electron acceptor D = electron donor Sac = sacrificial electron donor or acceptor  $k_r$  = radiative rate constant  $k_{nr}$  = non-radiative rate constant \* $E^{ox}$  =  $E(PS^{n+1}/PS^n)$ ,  $E^{ox}$  =  $E(PS^{n+1}/PS^n)$ \* $E^{red}$  =  $E(PS^n/PS^{n-1})$ ,  $E^{red}$  =  $E(PS^n/PS^{n-1})$ 

FIG. 1. Two major photo-induced electron transfer pathways.

quenching. As is also shown in Fig. 1, in a catalytic process a second redox reaction involving oxidized  $PS^{n+1}$  or reduced  $PS^{n-1}$  and a sacrificial redox reagent (Sac) is required to re-generate  $PS^n$ . Note that in a catalytic reaction which specific reagent is designated as the sacrificial reagent is context dependent, and sometimes, the sacrificial reagent is involved in the quenching step, with  $PS^{n+1}$  or  $PS^{n-1}$  then reacting

with the donor (D) or acceptor (A) substrate. But in any case, two sequential redox reactions are required to turnover PS<sup>n</sup> and render the photoinduced redox reaction catalytic.

### 2. Investigating mechanisms

Two major tools for mechanistic study of photocatalytic reactions are Stern-Volmer quenching analysis and transient absorption (TA) spectroscopy. Stern-Volmer quenching is one of the most convenient methods to evaluate electron transfer kinetics. That said, Stern-Volmer quenching on its own provides little mechanistic information because it does not distinguish electron transfer quenching from other quenching pathways, primarily energy transfer.<sup>14</sup> As a result, it is often necessary to conduct Stern-Volmer analysis in concert with other techniques, like TA, that distinguish energy transfer and electron transfer. However, once electron transfer is established as the dominant pathway, Stern-Volmer analysis is still very useful for measuring electron transfer kinetics and determining the kinetically preferred electron transfer pathway. There are two methods to evaluate the Stern-Volmer relationship, steady-state quenching, and time-resolved quenching. In steady-state quenching studies, the photoluminescence quantum yield  $(\Phi)$  is determined as the concentration of quencher is increased. More conveniently, the integrated steady-state emission intensity normalized to the absorbance at the excitation wavelength (I/Aex) is a suitable proxy for quantum yield. In timeresolved quenching studies, the photoluminescence lifetime  $(\tau)$  is measured. As the concentration of quencher increases, the photoluminescence lifetime decreases if \*PS<sup>n</sup> participates in a bimolecular reaction with the quencher. When each dataset is plotted and overlaid as depicted in Fig. 2, the type of quenching occurring, static or dynamic, can be determined. If dynamic quenching exclusively occurs, the excited-state photosensitizer and quencher react bimolecularly, and Stern-Volmer plots from both steady-state and time-resolved quenching data should have nearly identical linear trends as shown is Fig. 2(a). On the contrary, during static quenching [Fig. 2(b)] the quenching process takes place after a ground-state association between the quencher and the photosensitizer, not the excited state. In this type of scenario, the steady-state Stern-Volmer plot (photoluminescence

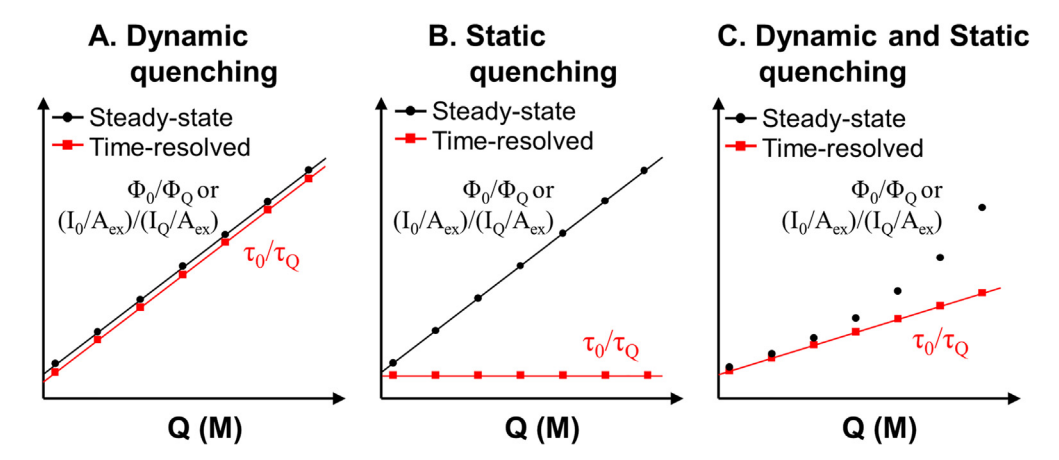


**FIG. 2.** Stern–Volmer plots based on different types of quenching mechanism.  $\Phi_0$  and  $\Phi_Q$  are the quantum yields, and  $\Phi_Q$  are the integrated steady-state emission intensities, and  $\Phi_Q$  are the photoluminescent lifetimes without and in the presence of quencher, respectively.  $\Phi_Q$  is the emission intensity at an excitation wavelength.

intensity) still shows the normal linear relationship, while timeresolved quenching study (excited-state lifetime) exhibits a flat line. If both dynamic and static quenching are involved in the mechanism [Fig. 2(c)], the time-resolved data appear linear and reflect the dynamic quenching component, whereas the steady-state data have a quadratic relationship that reflects a superposition of the static and dynamic quenching. The slope of a linear Stern-Volmer plot is known as the Stern-Volmer constant,  $K_{SV}$ , and it is equal to the product of the inherent excited-state lifetime and the bimolecular quenching rate constant,  $\tau_0 k_{\rm q}$ . Thus, in cases where the photosensitizer's lifetime is known, Stern-Volmer analysis can provide access to the quenching rate constant, which can be interpreted as an electron transfer rate constant if electron transfer is established as the dominant quenching pathway. In short, Stern-Volmer analysis provides important kinetic information for potential excited-state quenching pathways, but the mechanistic insight from Stern-Volmer alone is limited.

Transient absorption (TA) spectroscopy, also called timeresolved absorption spectroscopy, is a common technique for distinguishing energy transfer from electron transfer and for characterizing other mechanistic steps in a photocatalytic reaction beyond the primary quenching event. In TA, there are two types of light source as illustrated in Fig. 3. One is the white light probe source, and the other is a single wavelength pump laser that can excite the photoactive species. Using this pump-probe technique, excited-state spectral features, photogenerated intermediates, and their associated lifetimes can be observed, even when the species is not emissive.

Figure 4 briefly shows each step in a TA experiment with a sample that has a singlet ground state (S<sub>0</sub>) and two singlet excited states  $(S_1 \text{ and } S_2)$ . The ground-state absorption spectrum is obtained by the probe source [Figs. 4(a) and 4(d)]. When the pump pulse passes through the sample, a fraction of the molecules is promoted to the excited state S<sub>1</sub>, leading to a high and non-equilibrium population [Fig. 4(b)]. Then, a weak probe pulse passes through the sample again with a time delay t with respect to the pump pulse [Fig. 4(c)]. The difference between the excited-state absorption spectrum and the ground-state absorption spectrum is then calculated ( $\Delta OD_t$ ), resulting in the spectrum as shown in Fig. 4(f). In regions where the ground-state absorption is greater than the excited-state absorption, a ground-state bleach (negative  $\Delta OD_t$ ) is observed. In regions where the excited-state absorption is greater than the ground-state absorption, a growth (positive  $\Delta OD_t$ ) is observed. Providing that there is no irreversible excited-state chemistry occurring, the  $\Delta OD_t$  spectrum reaches zero at long enough time scale since the excited-state sample relaxes back to the ground state. By measuring the TA spectra with different

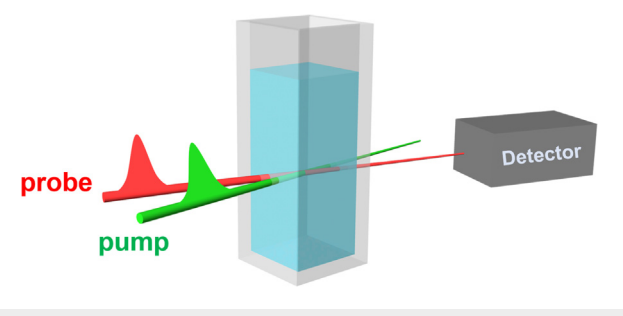


FIG. 3. Schematic representation of transient absorption (TA) spectroscopy.

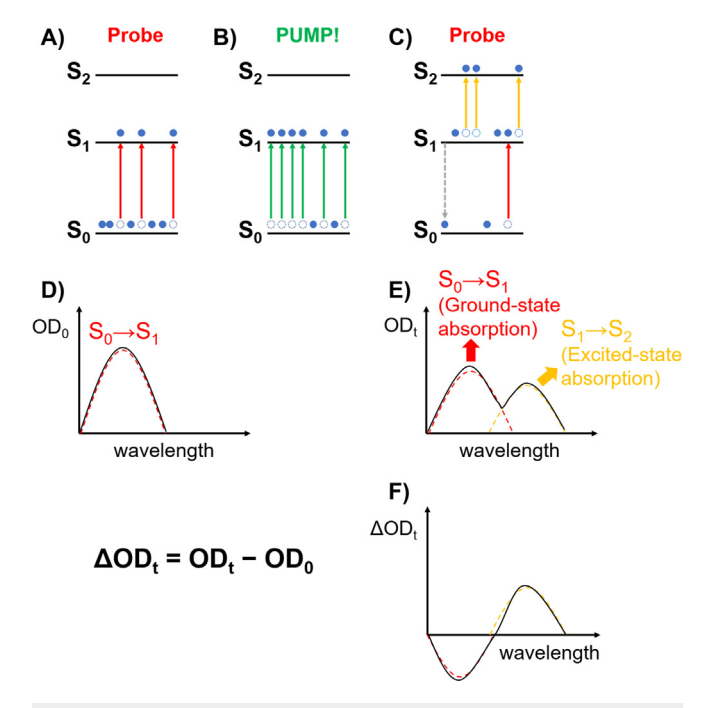


FIG. 4. Process of TA spectroscopy.

time delays, the excited-state lifetime and the timescales of any quenching events can be obtained.

As a representative example of how to distinguish energy transfer and electron transfer, we consider the ubiquitous example of  $[Ru(bpy)_3]^{2+}$  (bpy = 2,2'-bipyridine). When the metal-to-ligand charge transfer (MLCT) excited state of  $[Ru(bpy)_3]^{2+}$  is quenched, the resulting chemical species depends on whether the quenching occurs via energy transfer, oxidative quenching, or reductive quenching. The MLCT excited state of  $[Ru(bpy)_3]^{2+}$  can be formulated as  $[Ru^{III}(bpy)^{\bullet-}(bpy)_2]^{2+}$ . If energy transfer occurs,  $[Ru^{III}(bpy)^{\bullet-}(bpy)_2]^{2+}$  is transformed back to  $[Ru(bpy)_3]^{2+}$ . However, through electron transfer,  $[Ru^{III}(bpy)^{\bullet-}(bpy)_2]^{2+}$  will donate or accept one electron, resulting in  $[Ru^{III}(bpy)_3]^{3+}$  or  $[Ru^{II}(bpy)^{\bullet-}(bpy)_2]^+$ , which exhibit different absorption features. Moreover, in some cases the quencher molecule has visible TA features for its excited state and/or reduced and oxidized forms, which can additionally be probed to provide further evidence for the quenching pathway.

This review article does not extensively cover Stern-Volmer quenching and TA spectroscopy and their applications in mechanistic studies of photoinduced redox reactions, but it is important to recognize that many of the electron transfer pathways and redox intermediates that are discussed throughout this review were characterized using these techniques.

# B. Photophysical and electrochemical properties

The major focus of this review is strategies for accessing exceptionally strong excited-state reductants and oxidants. As such, the redox potentials, particularly those from the excited state, are critical metrics for evaluating the reducing or oxidizing power of a photosensitizer. These redox potentials determine the thermodynamic limits of

excited-state electron transfer for a photosensitizer and, as described in Sec. II A, are critical determinants of the kinetics of electron transfer as well. This section defines the relevant redox potentials and summarizes how they are determined.

#### 1. Excited-state energy

When photosensitizers or photocatalysts are promoted to an electronically excited state after absorbing visible light, they will rapidly relax to the lowest vibrational energy level prior to any quenching occurring. In organic photosensitizers, the operative excited state is often a singlet state, abbreviated as S<sub>1</sub>, although crossover to the lowest triplet state, T1, can occur in some cases. For metal-based photosensitizers, T<sub>1</sub> is almost always the relevant excited state. The energy difference between the ground states So and So or To is the excited-state energy, which is usually termed  $E_{0,0}$ . There are different ways to estimate  $E_{0.0}$ . The first method is a spectroscopic estimation using normalized UV-Vis absorption and photoluminescence emission spectra measured at room temperature. When both spectra are overlaid, the intersection point of those two spectra can be determined as the excited-state energy, providing the overlapping bands represent absorption and emission transitions of the same electronic origin. If the photocatalyst is not emissive at room temperature or there is no clear crossing point between the two spectra, the maximum wavelength of the first vibronic peak of the photoluminescence spectrum obtained at low temperature, usually 77 K, can be assigned as  $E_{0,0}$ value. 35,36 Another simple method is to use the position of the longwavelength tail of the absorption spectrum to predict  $E_{0,0}$ . Finally, it is possible to estimate  $E_{0,0}$  values computationally using density functional theory (DFT) and time-dependent density functional theory (TD-DFT).3

#### 2. Ground- and excited-state redox potentials

The most common method to determine ground-state redox potentials is to use cyclic voltammetry. Using cyclic voltammograms, the ground-state oxidation potential  $E^{\rm ox}$  (reduction potential  $E^{\rm red}$ ) is determined as the potential where the first one-electron oxidation (reduction) occurs. For chemical species that exhibit reversible redox features, the value can be determined using Eq. (5). The calculated value is also known as the half-wave potential ( $E_{1/2}$ ),

$$E_{1/2} = \frac{1}{2} \times (E_{pc} + E_{pa}). \tag{5}$$

In Eq. (5),  $E_{\rm pc}$  is the cathodic peak potential and  $E_{\rm pa}$  is the anodic peak potential. In the case of irreversible redox waves,  $E_{\rm pc}$  or  $E_{\rm pa}$  can be assigned as  $E^{\rm red}$  or  $E^{\rm ox}$ , or alternatively, the onset potential ( $E_{\rm onset}$ ), suggested by Vullev et al., <sup>43</sup> can also be assigned as  $E^{\rm red}$  or  $E^{\rm ox}$ .

#### 3. Excited-state redox potential

Based on the estimated excited-state energy and the measured ground-state redox potentials, the excited-state redox potentials can be calculated using Eqs. (6a) and (6b). Strictly speaking, these equations neglect the entropy difference between the ground state and the excited state and coulombic effects of charge separation, but they are nonetheless good estimates for excited-state redox potentials and are very commonly used,

$$^*E^{red} = E^{red} + E_{0,0},$$
 (6a)

$$^*E^{ox} = E^{ox} - E_{0.0}.$$
 (6b)

To avoid confusion, here we will describe the use of terms reduction potential ( $E^{red}$ ), oxidation potential ( $E^{ox}$ ), excited-state reduction potential (\* $E^{\text{red}}$ ), and excited-state oxidation potential (\* $E^{\text{ox}}$ ). Even though two of these values are termed "oxidation potentials," they all refer to thermodynamic potentials of the corresponding reduction half reaction. For example, the oxidation potential (Eox) of D represents the formal potential of the reduction half reaction  $D^{\bullet+} \rightarrow D$ . In another example, the excited-state oxidation potential of A is defined by the reductive half reaction A<sup>•+</sup>→\*A. Most importantly, the reader should internalize what these relative values mean. From the standpoint of the photosensitizer, a more positive value of \*E<sup>red</sup> means that the photosensitizer is a stronger photooxidant, and a more negative value of \*E<sup>ox</sup> implies that the photosensitizer is a stronger photoreductant. For potential electron donors (D) or acceptors (A) that can react with photosensitizer, a more positive  $E^{ox}$  value for the donor means it is more difficult to oxidize, and a more negative  $E^{\text{red}}$  value for the acceptor means it is more difficult to reduce.

Figure 5 illustrates schematically how excitation increases the oxidizing or reducing power of the photosensitizer, by an amount equal to  $E_{0,0}$ . Also shown in Fig. 5, in order for thermodynamically favorable reductive quenching to occur, \* $E^{\rm red}$  of the photosensitizer must be more positive than  $E^{\rm ox}$  of the donor, and for thermodynamically favorable oxidative quenching, the photosensitizer's \* $E^{\rm ox}$  must be more negative than the acceptor's  $E^{\rm red}$ .

In molecular photosensitizers, excited-state redox potentials are typically measured relative to the lowest vibrational energy level of the lowest-energy electronic excited state (normally  $S_1$  or  $T_1$ ). This lowest-energy state is rapidly accessed through non-radiative relaxation following excitation. However, it is worth noting that in some cases charge transfer can occur from a higher-lying electronic or vibrational states, effectively increasing the excited-state redox potential for that electron transfer event. This electron transfer process, often referred to as "hot" injection, is relevant in dye-sensitized solar cells (DSSC) where interfacial electron transfer is occurring between a dye and semiconductor,  $^{44-48}$  but is not relevant to bimolecular excited-state electron transfer.

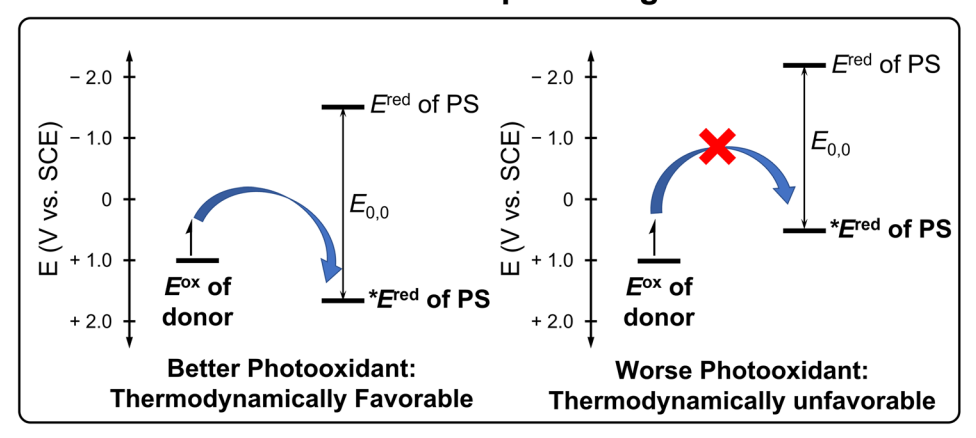
In the field of photoredox catalysis, the electrochemical potentials are usually referenced against the saturated calomel electrode (SCE). Therefore, all redox potentials presented in this review are referenced to SCE unless otherwise noted, for convenient comparison to many other resources. Some of data are reported directly from the original work, and the others are adjusted to the SCE scale using well-established conversion tables. <sup>49,50</sup>

# III. STRATEGIES FOR HIGHLY REDUCING AND OXIDIZING PHOTOSENSITIZERS

#### A. Molecular design approaches

The oxidizing and reducing abilities of photosensitizers are closely related to the energy levels of the frontier orbitals, which dictate the ground-state redox potentials and are a determining factor of the excited-state energy. Controlling frontier orbital energies, therefore, is critically important for designing potent photosensitizers. Most common photosensitizer classes are conjugated organic molecules or coordination compounds with conjugated ligands. As such, the most

# Reductive quenching



# Oxidative quenching

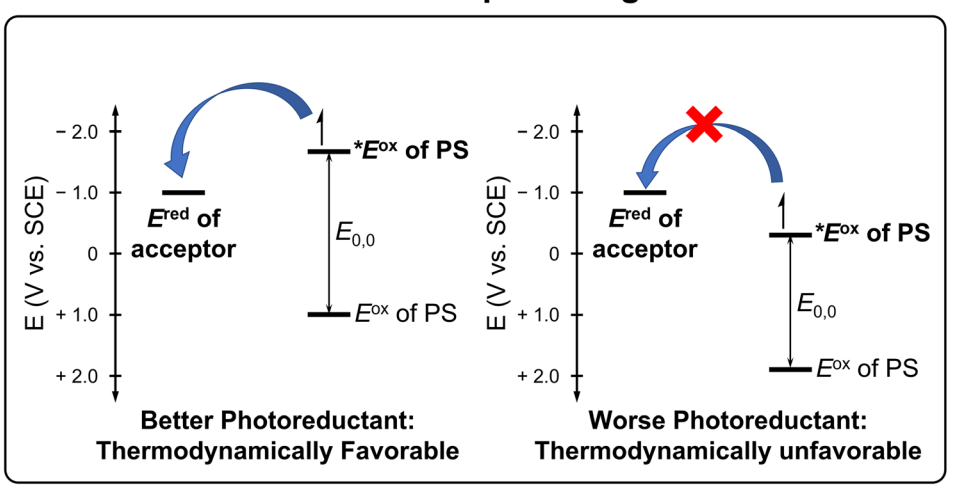


FIG. 5. Relative energy level diagram showing thermodynamically favorable or unfavorable reductive and oxidative quenching processes.

widely used method to perturb frontier orbital energies has been to incorporate electron-withdrawing or electron-donating groups to the molecule or to extend  $\pi$ -conjugation.<sup>20</sup>

In this part, we will focus on structural modifications that result in extreme redox potentials, with examples of both organic molecules and metal-based photosensitizers provided. We do note that there are other classes of photosensitizers that are fundamentally and technologically important, but do not quite meet the criteria for "extreme" redox potentials we have outlined above. For example, platinum acetylide photosensitizers<sup>51</sup> have been extensively developed and were important in a lot of early solar fuel research. 52,53 In addition, porphyrin and other polypyrrole photosensitizers are very prominent in photochemistry research, 54,55 but they generally do not qualify as extreme photoredox agents. Recent work has shown that peripheral substitution to porphyrin cores can render them rather strong ground-state oxidants, <sup>56</sup> although the modest excited-state energies of porphyrins limits their excited-state reducing and oxidizing power. For a thorough listing of photosensitizer properties, we refer the reader to a comprehensive review from our group that tabulates the relevant redox

properties of more than 200 photosensitizers commonly used in photoredox catalysis.  $^{22}$ 

#### 1. Acridinium chromophores

Since Fukuzumi's work on compound 1 (9-mesityl-10-methylacridinium perchlorate, Fig. 6), which demonstrated a strongly oxidizing charge-separated state after excitation and an exceptional excited-state reduction potential (\* $E^{\rm red}$ ) of +2.06 V, <sup>57,58</sup> acridinium-based photosensitizers have been widely studied in many photoin-duced reactions, which require a strong oxidant. <sup>18,59,60</sup> In the context of photoredox catalysis for organic synthesis, Joshi-Pangu *et al.* developed a series of acridinium photocatalysts **2–6**, which demonstrate structure–property relationships in this class of photosensitizers. <sup>61</sup> They incorporated electron-donating *tert*-butyl and methoxy groups to the acridinium core to achieve more negative ground-state reduction potentials. All acridiniums **2–6** have more negative  $E^{\rm red}$  value (-0.57 to -0.84 V) compared to **1** (-0.57 V) and are similar or slightly weaker as photooxidants (\* $E^{\rm red}$  = +1.65–+2.08 V, compared

FIG. 6. Structures of acridinium photosensitizers.

to +2.06 V). Unlike compound 1, the N-aryl analogues 2-6 are effective photosensitizers for the decarboxylative conjugate addition of Cbz-proline to dimethyl maleate, attributed in large part to the enhanced stability afforded by replacing the N-methyl group in 1 with an aryl substituent.

In subsequent work, White, Wang, and Nicewicz further explored the systematic control of photophysical and redox properties of acridiniums, separately modifying substituents located on the acridinium core, the 9-position of this core, or the acridinium nitrogen (7-22). Based on the observed trends, they synthesized 22 by selecting the best-performing elements from each category, and 22 shows not only an enhanced  $^*E^{\rm red}$  of  $+2.20\,{\rm V}$  but also a longer excited-state lifetime.

Fischer and Sparr elaborated synthetic methods of acridinium ions, which have electron-donating groups on the acridinium <sup>3,64</sup> With this series of substituted acridiniums (23–34), the same authors collaborated to demonstrate tunability of the excited-state oxidative character.<sup>65</sup> They introduced NMe<sub>2</sub> and/or OMe groups to the acridinium core and used phenyl, mesityl, xylyl, and 1-naphthyl as the nine-position substituent. Compounds 27 and 28, which have the most positive excited-state reduction potentials in the series (+1.69 and +1.73 V, respectively), exhibit the best catalytic activity in a decarboxylative fluorination reaction. Alemán, Mancheño, and coworkers introduced polar imide group to the nine-position of acridinium (35 and 36). These substituted acridinium photocatalysts have \*E<sup>red</sup>  $\sim +2.4 \, \text{V}$ , substantially more positive values than that of 1 (+2.18 V), and on account of their stronger oxidizing properties in the excitedstate outperform 1 in the dehydrogenative lactonization of 2-phenylbenzoic acid.

#### 2. Cyanoarenes

Cyanoarenes, which have an aromatic core and one or more cyano substituents as shown in Fig. 7, are one of the most thoroughly studied organic photosensitizers due to their wide ground-state redox potential windows (from -0.7 to -1.7 V for the reduction potentials and about +1.5 V for the oxidation potentials) and their structural tunability. The simplest structural modification for controlling redox potential of cyanoarenes is to extend conjugation or to introduce electron-donating or electron-withdrawing substituents to the aromatic ring (37-51).  $^{69-71}$ 

The cyanoarene class was expanded by the Zhang<sup>72,73</sup> and Zeitler groups.<sup>74</sup> They prepared carbazolyl or diphenylamino (DP) dicyanobenzene derivatives, which have donor-acceptor (D-A) molecular dyad structures (52-65). With this structural design, the carbazolyl (Cz) or diphenylamino (DP) moiety and the dicyanoarenes can be electron donors and acceptors, respectively. Therefore, modifying the number or position of carbazolyl or diphenylamino group or incorporating various substituents onto the center benzene ring can control the HOMO and LUMO energy levels. Among the series of cyanoarenes, 1,2,3,5-tetrakis(carbazol-9-yl)-4,6-dicyanobenzene (4CzIPN, 52) has been widely used<sup>67,75–83</sup> due to its well-balanced ground- and excitedredox potentials ( $E^{\text{red}} = -1.24 \text{ V}, E^{\text{ox}} = +1.49 \text{ V}, *E^{\text{red}} = +1.43 \text{ V},$ and  ${}^*\hat{E}^{\rm ox} = -1.18\,{\rm V}).^{74}$  These potentials suggest that 4CzIPN is a strong excited-state oxidant and a moderately strong excited-state reductant, making it a versatile photosensitizer candidate for a variety of photoinduced redox transformations. Using 52 as a starting point, Zeitler and coworkers demonstrated a systematic alteration of redox potentials of cyanoarenes.<sup>74</sup> Introducing chlorine to the cyanoarene core (59) induces stronger oxidizing properties by increasing the ground-state oxidation potential ( $E^{ox} = +1.79 \,\mathrm{V}$ ). By contrast, incorporating electron donating methoxy-carbazol (65) leads to increase in

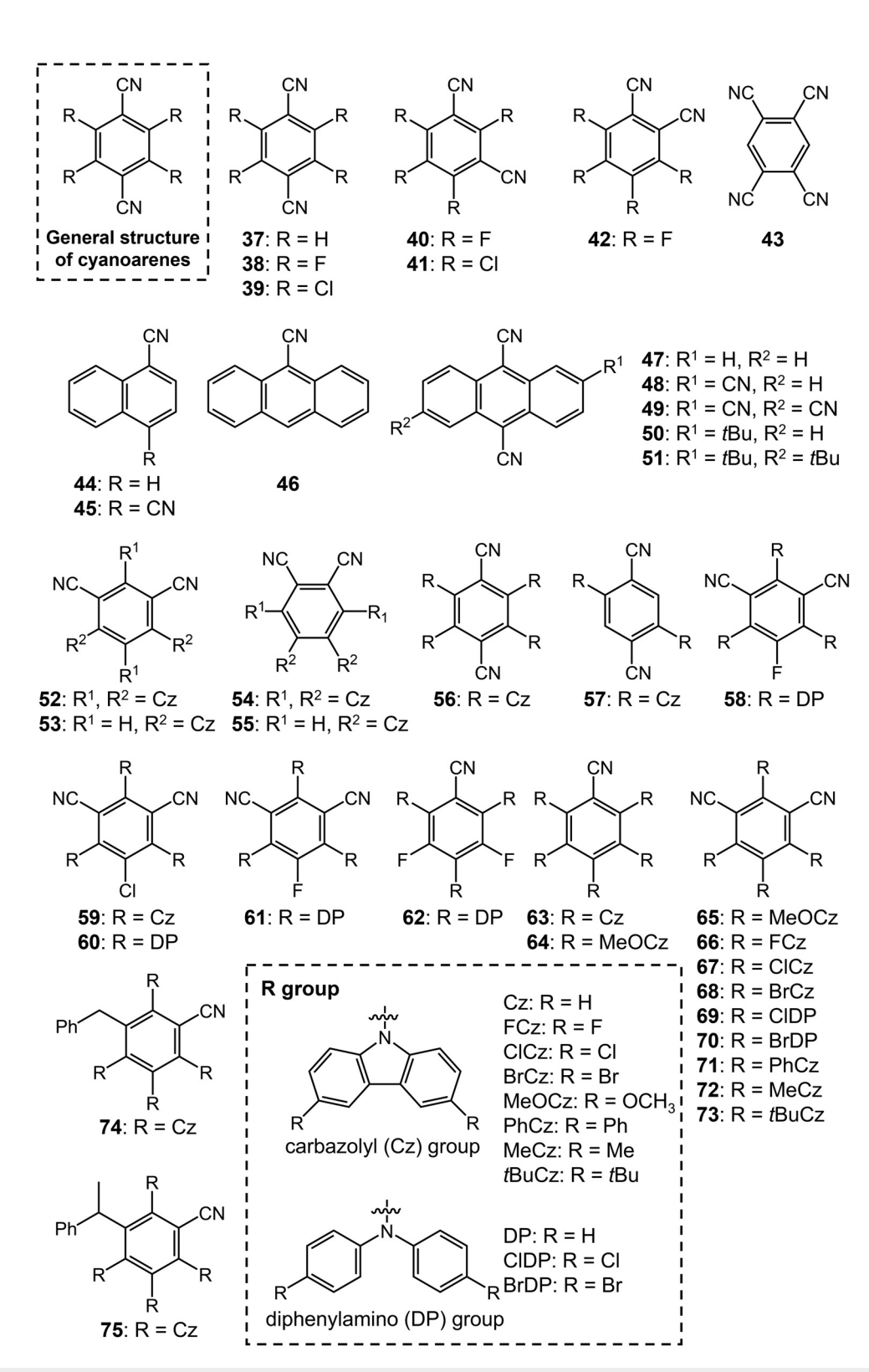


FIG. 7. Structures of cyanoarene photosensitizers.

the reducing power ( $E^{\rm red}=-1.34\,{\rm V}$ ). With the combination of donor-based effects and acceptor core-related modifications, they showed that **62** has a very negative ground-state reduction potential ( $E^{\rm red}=-1.92\,{\rm V}$ ) and outperformed other cyanoarene photocatalysts in the reductive C–O bond cleavage reaction of lignin model substrates and in the photocatalytic reductive detriflation of aryl triflates.

Waser and coworkers  $^{84,85}$  and Yu and coworkers  $^{86}$  demonstrated with compounds **65–73** that substituents on the Cz or DP can modulate  $^*E^{\rm red}$ . Electron-donating groups decrease the excited-state oxidizing power (less positive  $^*E^{\rm red}$ ) and electron-withdrawing halogen substituents increase the excited-state oxidizing power (more positive  $^*E^{\rm red}$ ). Halogen-substituted **66–68** have more positive excited-state reduction potential than **52** and show higher photocatalytic activity in the synthesis of alkynyl nitriles.  $^{84}$  Compounds **74** and **75**, which are the degradation products of **52** formed by radical addition of the benzyl (**74**) or phenylethyl (**75**) radical, were isolated by the König group and reported in 2019.  $^{87,88}$  One cyano group of **52** was replaced with a benzyl or phenylethyl group during the catalytic reaction, and it was found that the radical anions of **74** and **75** have reasonably negative ground-state reduction potentials of -1.72 and -1.69 V, respectively.

#### 3. Phenazine, phenoxazine, and phenothiazine

The two above classes of organic photosensitizers are particularly noted for their highly oxidizing excited states, though there are other classes of organic molecules, which are strong photoreductants. In polymer chemistry, controlled radical polymerizations (CPRs) are critical to synthesize polymers with predictable molecular weights (MWs) and narrow MW distribution.<sup>89</sup> Phenazine, phenoxazine, and phenothiazine are structurally related classes of organic photosensitizers, which are widely used in CPRs due to their highly reducing excitedstate potentials. 16,90-92 The Miyake group presented a series of phenazine-based photocatalysts (76-91, Fig. 8). 93-95 In 2016, they introduced diaryl dihydrophenazines, functionalizing the phenyl substituents. 93 The triplet excited-state oxidation potential was controlled by functionalization of the phenyl substituents. Introducing electron withdrawing groups (78, 79) induces less negative  ${}^*E^{\text{ox}}$ , but the addition of electron-donating OMe groups (76) results in a slightly more negative  $^*E^{\text{ox}}$  value of  $-2.36\,\text{V}$ , compared to 77 ( $-2.34\,\text{V}$ ). In the next work, they used various N-aryl substituents (76-78, 80-85). 94 Of the nine phenazine photocatalysts, 81 has the most negative calculated \* $E^{\text{ox}}$  value, reported as  $-2.28\,\text{V}$  in this work. They also demonstrated redox potential control by the incorporation of aryl groups to the phenazine core. 95 Compounds with methoxyphenyl (90) or dimethylaminophenyl (91) groups retain strongly reducing  $E^{ox}$  values (-2.12) and −2.15 V, respectively). Miyake and coworkers also demonstrated highly tunable photophysical and electrochemical properties of phenoxazines via systematic structural modification of the N-aryl moiety and core substituents (92–110). 96–98 The triplet excited-state oxidation potentials of phenoxazines with electron-donating methoxy (99, 104) or diphenyl amino (107) substituents were determined to be -2.01, -1.91, and -1.88 V, respectively, exhibiting strong reducing properties. N-trifluoromethylphenyl phenoxazines, which have strong excited-state oxidation potentials, were presented by Son, Cho, and coworkers (93, 111-114).  $^{99,100}$  The estimated  $^*E^{ox}$  value of 111 is -2.56 V, which is the most negative excited-state oxidation potential in the series. Due to the strong reducing power of 111, it can reduce

FIG. 8. A series of phenazine, phenoxazine, and phenothiazine.

unactivated aryl halides to aryl radical intermediates and was used as a photocatalyst in C–C and C–B bond-forming reactions.  $^{100}$  Phenothiazine-based compounds are one of the traditionally used photoredox catalysts due to their low cost, readily availability, and facile modification.  $^{101,102}$ 

After Hawker and coworkers demonstrated photocatalytic activity of parent phenothiazine 115 in atom transfer radical polymerization (ATRP) reactions,  $^{103}$  phenothiazine-based photocatalysts have been extensively used in this area.  $^{104-118}$  Although there are some references that presented structural modification of phenothiazine,  $^{104-109,113}$  most of their excited-state oxidation potentials are not more negative than 115 ( $-2.1\,\mathrm{V}$ ), except a few cases.  $^{104,105}$  In 2016, Matyjaszewski group presented a series of phenothiazines (115–121), and the  $^*E^{\mathrm{ox}}$  value of 119 is determined to be  $-2.23\,\mathrm{V}$ , which is more negative than 115.  $^{104}$  Larionov and coworkers used four phenothiazines (115, 120–122) in photocatalytic borylation reactions of C–O, C–N, and C–X bonds.  $^{105}$  Compound 122 has  $^*E^{\mathrm{ox}}=-2.71\,\mathrm{V}$  and showed an improved catalytic performance in the borylation of aryl phosphates.

#### 4. Ru(II) and Ir(III) complexes

Metal-based coordination complexes, which are composed of a transition metal surrounded by conjugated visible-light-absorbing ligands, also have been actively developed in many photocatalytic applications. Although concerns about materials cost and metal toxicity have motivated the development of "metal-free" organic photosensitizers like those described in Secs. III A 1-III A 3, it is still true that several classes of metal-based photosensitizers are the top performers in several applications, on account of their broad and intense visible absorption, long-lived charge-separated states, and tunable redox potentials that enable the design of potent photoreductants and photooxidants. In the fields of photovoltaics and photocatalysis, ruthenium(II) polypyridyl complexes are the most commonly studied molecular photosensitizers among photoactive late-transition metal Ru(II) complexes were initially used in water splitting 121,122 and applications in photonic and optoelectronic devices. 123 With pioneering research by MacMillan, 124 Yoon, 125 and Stephenson's groups, 126 a series of common homoleptic Ru(II) complexes (123–128, Fig. 9) have also been used in many organic synthesis applications. 8,9,11,12,127–129 However, the excited-state oxidation potential of  $[Ru(bpy)_3]^{2+}$  (\* $E^{ox} = -0.81 \text{ V}$ ) is insufficiently negative to initiate redox reactions with many classes of unactivated organic substrates. Furthermore, for 127 and 128, not only can single electron transfer occur in the excited state, but proton coupled electron transfer (PCET) is also possible because the basicity of the peripheral nitrogen atoms of 2,2'-bipyrazine and 2,2'-bipyrimidine increase in the MLCT excited state. 130-133 In PCET, electron transfer and proton transfer occur consecutively or concertedly, and there are many reports of excited-state PCET that involve charge-transfer excited states. Although detailed mechanistic aspects will not be discussed further here, PCET is one of the most important charge transfer mechanisms in photocatalytic reactions. 13

Cyclometalated iridium photosensitizers, also summarized in Fig. 9, are much better suited for challenging reductive transformations than their ruthenium counterparts. In 2012, Stephenson and coworkers successfully demonstrated photocatalytic dehalogenation of alkyl, alkenyl, and aryl iodide substrates using *fac*-Ir(ppy)<sub>3</sub> (129), which has a much more negative  $^*E^{\text{ox}}$  value of  $-1.73\,\text{V}$  compared to Ru(bpy)<sub>3</sub> $^{2+}$ .  $^{139}$ 

MacMillan's group, in 2018, introduced electron-donating methoxy and *tert*-butyl groups to the 2-phenylpyridine (ppy) ligand in

a series of homoleptic complexes (130–137). Although their research focused on the relationship between the ground-state oxidation potential ( $E^{\rm ox}$ ) and enantioselectivity of  $\alpha$ -benzylation of aldehydes, the excited-state oxidation potentials of all of these substituted Ir(III) complexes are more negative ( $<-1.73~\rm V$ ) than that of fac-Ir(ppy)<sub>3</sub>. Wenger and coworkers presented new sulfonated variants of fac-Ir(ppy)<sub>3</sub> (138–141) to increase solubility in water, and these modifications also result in more reducing excited states than fac-Ir(ppy)<sub>3</sub> (\* $E^{\rm ox}=-1.85,-1.76,$  and  $E^{\rm ox}=-1.85,$  1.76, and  $E^{\rm ox}=-1.85,$  1.76, and  $E^{\rm ox}=-1.85,$  1.76, and 1.94 V for 138, 139, 140, and 141, respectively).

Cyclometalated iridium complexes can also be engineered to be strong photooxidants. Bernhard and coworkers have presented extensive research on cationic heteroleptic Ir(III) complexes, shown in Fig. 10, which have two organometallic cyclometalating ligands and one neutral bidentate ligand, usually from the 2,2'-bipyridine family. 144-146 These heteroleptic Ir(III) complexes are not particularly strong photoreductants, with similar excited-state reducing power as  $[Ru(bpy)_3]^{2+}$ . However, they do show stronger oxidizing power (\* $E^{red}$  $= +0.70-+0.97 \,\mathrm{V}$ ) in the excited-state compared to  $[\mathrm{Ru}(\mathrm{bpy})_3]^{2+}$ (\* $E^{\text{red}} = +0.68 \text{ V}$ ), and their combined redox properties and exceptional stability have made them very popular and versatile choices for photoredox organic methology.<sup>11</sup> In 2016, Knowles and coworkers synthesized five heteroleptic Ir(III) complexes (142-146) using dF(CF<sub>3</sub>)-ppy (2-(2,4-difluorophenyl)-5-trifluoro-methylpyridine) as the cyclometalating ligand and bipyridine derivatives as the neutral chelate. 147 The excited-state reduction potentials (\*E<sup>red</sup>) of all Ir(III) complexes in this series are more positive than [Ru(bpy)<sub>3</sub>]<sup>2+</sup>. Compounds 145 and 146, which have electron-withdrawing CF<sub>3</sub> groups on the bipyridine, exhibit robust photocatalytic activity in C-H alkylation reactions due to their strongly oxidizing excited-state potentials of +1.65 and +1.68 V, respectively.

To push the limits for extreme excited-state redox potentials and expand the substrate scope for reductive photoredox transformations, our group has developed a series of heteroleptic Ir(III) complexes (147–165) supported by electron rich  $\beta$ -diketiminate (NacNac) ligands, which are potent excited-state reductants (Fig. 10). 36,148-The electronic characteristics of the NacNac can be readily modulated by its substitution pattern. Making the NacNac more electron-rich progressively destabilizes the HOMO energy level and results in more negative values of the ground-state redox potentials, making these Ir(III) complexes more powerful photoreductants.<sup>36</sup> All Ir(III) complexes with pyridine- or pyrazole-based cyclometalating ligands (147-159) exhibit excited-state oxidation potentials more negative than  $-2.0 \,\mathrm{V}$ , which represent  $300-500 \,\mathrm{mV}$  more reducing power than fac-Ir(ppy)<sub>3</sub> (\* $E^{ox} = -1.73 \text{ V}$ ). Owing to their potent excited-state reducing power, 148 and 155 show photocatalytic activity not only in hydrodebromination of aryl bromide substrates, 36,149 but also dehalogenation of other challenging substrates such as aryl chlorides, aryl fluorides, and alkyl bromides. 149 All of 147-159 have a narrow range of excited-state oxidation potentials (-2.0--2.2 V), motivating our group to introduce triazole and NHC-based complexes 160-165 to break through the  $-2.2 \,\mathrm{V}$  ceiling. <sup>150</sup> Incorporation of these alternative cyclometalating ligands increases the LUMO energy levels and tripletstate energies, resulting in the even more potent cyclometalated Ir(III) photoreductants [see Eq. (6b)]. The excited-state oxidation potentials of 160 and 164 are  $-2.4 \,\mathrm{V}$ , which is 700 mV more negative than fac- $Ir(ppy)_3$ .

FIG. 9. Ru(II)- and Ir(III)-based photocatalysts.

Ancillary ligand modification can also increase visible-light absorption and maximize photooxidation capabilities. In 2020, Troian-Gautier and coworkers reported three Ir(III) complexes as strong photooxidants with intense visible absorption (166–168). Introducing two trifluoromethyl substituents on the 2-phenylpyridine ligands increases the excited-state oxidizing power of these

photosensitizers. The excited-state reduction potential values of **166**, **167**, and **168** are +1.54, +1.53, and +1.52 V, respectively, and these values are 1.2 V more positive than fac-Ir(ppy)<sub>3</sub> (\* $E^{\rm red}$  = +0.35 V), and 0.8 V more positive than  $[{\rm Ru}({\rm bpy})_3]^{2+}$  (\* $E^{\rm red}$  = +0.68 V). Extending the  $\pi$ -conjugation system of the ancillary N^N ligand stabilizes the LUMO energy level, increasing visible-light absorption.

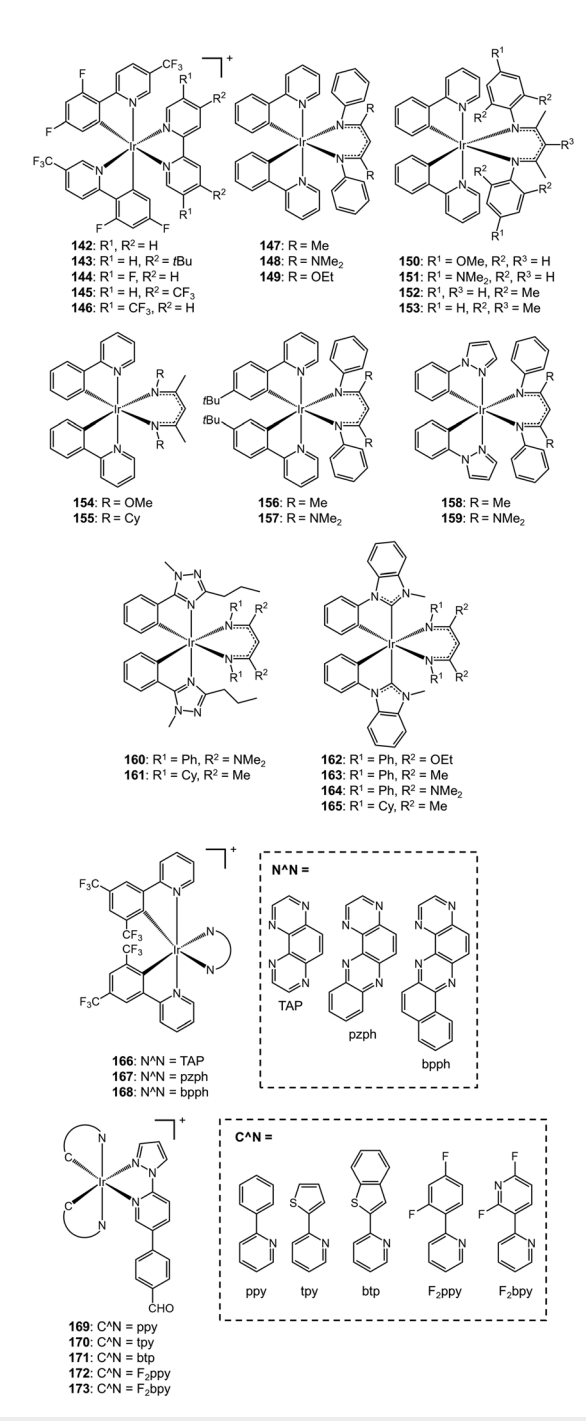


FIG. 10. Heteroleptic Ir(III) complexes.

Zhu, Tan, Su, and coworkers demonstrated photocatalytic hydrogen generation using cationic  $[Ir(C^N)_2(ppba)](PF_6)$  complexes [169–173, ppba = 4-(6-(1H-pyrazol-1-yl)pyridine-3-yl)benzalde-hyde]. Incorporating electron-withdrawing fluorine atoms on the C^N ligands (172 and 173) results in a more positive excited-state reduction potential,  $+1.06\,\mathrm{V}$  for 172 and  $+1.16\,\mathrm{V}$  for 173 (potentials

were originally reported vs NHE,  $+1.30\,\mathrm{V}$  for 172 and  $+1.40\,\mathrm{V}$  for 173). The oxidation potential of triethylamine (TEA),  $E(\mathrm{TEA}^+/\mathrm{TEA})$ , is  $+0.69\,\mathrm{V}$  ( $+0.93\,\mathrm{V}$  vs NHE), so the potential difference between TEA and the excited state of 172 and 173 provides the driving force for photocatalytic hydrogen generation, allowing electron transfer between the two species.

#### 5. Other metal complexes

Platinum(II) complexes are another widely researched class of photoactive transition metal compounds, 153-159 though not as widely used as Ru(II) or Ir(III) complexes in photocatalytic applications. Che's group developed tetradentate Pt(II) complexes with strong excited-state reducing properties. 160-162 In 2018, they demonstrated photocatalytic reductive coupling of aromatic carbonyls and hydrodebromination of aryl bromides using Pt(II) complexes supported by bis(phenolate-NHC) ligands (174-176, Fig. 11). 163 The excited-state reduction potential of 175, which has electron-donating carbazolyl groups incorporated into the bis(phenolate-NHC) ligand, is calculated to be  $-2.18\,\mathrm{V}$ , and this value is comparable to other potent photoreductants. Due to its strong excited-state reducing power, 175 shows a good photocatalytic activity in reductive coupling of aromatic carbonyl compounds and reductive hydrodebromination of aryl bromide substrates. One limitation of 174-176 is that they only absorb in the UV region, requiring excitation at  $\lambda < 400$  nm to operate. Fukuzumi, Cho, You, and coworkers investigated photoredox catalytic trifluoromethylation reaction using Pt(II) complexes with anionic cyclometalating C^N ligands (177–179). 164 The anionic cyclometalating ligand can induce cathodic shifts of the excited-state redox potential, so these Pt(II) complexes are likewise potent photoreductants with excitedstate oxidation potentials of -2.11 V for 177, -2.07 V for 178, and  $-1.93 \,\mathrm{V}$  for 179. Specifically, 178 exhibits excellent catalytic performances in trifluoromethylation of alkenes and heteroarenes.

Even though Ru(II), Ir(III), and Pt(II) complexes have been widely used in many photoredox catalytic reactions, those metals have limitations of high price and scarcity. Therefore, the development of cheaper, earth-abundant transition metal complexes is important for sustainable large-scale applications. Cu(I) is one of the promising candidates due to its low price and abundance. Moreover, unlike most other 3d metals its d<sup>10</sup> configuration means there are no low-lying ligand-field excited states that deactivate the longer-lived, redox-active charge-transfer states. In 2005, Peters and coworkers described an amido-bridged bimetallic [(PNP)Cu]<sub>2</sub> system (180), where PNP is bis(2-(diisobutylphosphino)phenyl)amide. 165 Due to strong phosphine donors, the Cu<sup>1.5</sup>/Cu<sup>1.6</sup>/Cu<sup>1</sup> redox potential shifts cathodically when compared to previously reported [(SNS)Cu]2 complexes [SNS = bis(2-tert-butylsulfanylphenyl)amide]. 166 The excited-state oxidation potential of 180 is calculated to be  $-2.74 \,\mathrm{V}$ , making it one of the most potent photoreductants known.

Collins' group presented a comprehensive work preparing 50 Cu(I) complexes including 40 heteroleptic complexes (181–220) and 10 homoleptic complexes derived from diimine and bisphosphine ligands.  $^{167}$  By using different kinds of bisphosphine ligands to vary the nature of chromophore and bite angle, they can control the photophysical properties and catalytic activity of Cu(I) complexes. The values of the excited-state oxidation potentials ( $^*E^{\text{ox}}$ ) of the Cu(I) complexes are between approximately -1.3 and  $-1.9\,\text{V}$ , and

FIG. 11. A series of Pt(II) and Cu(I) complexes.

complexes with BINAP and Xantphos ligands exhibit the most negative potentials. Thus, some members of this series are strong photoreductants with potentials that rival some of the homoleptic iridium complexes like *fac*-Ir(ppy)<sub>3</sub> (129).

In 2019, Poisson and coworkers reported photocatalyzed borylation of aryl, heteroaryl, vinyl, and alkyl halides using heteroleptic Cu(I) complexes including **221** and **222**. The excited-state oxidation potential of **221** is  $-1.92\,\mathrm{V}$ , and its potent excited-state reducing power makes borylation reactions of iodo- and bromoarenes and heteroarenes, which involve electron transfer to the organohalide substrates, possible.

Homoleptic group 6 transition metal complexes [Cr(0), Mo(0), and W(0)], supported by isocyanide ligands, have been comprehensively studied by Gray's group 168-170 and Wenger's group 171-173 as a promising class of strong photoreductants. In 2013, Gray and coworkers reported homoleptic arylisocyanide W(0) complexes (223 and 224, Fig. 12). 168 These W(0) complexes contain bulkier dimethylphenyl and diisoproylphenyl isocyanide ligands, which protect the metal center and prevent excited-state decay. Complex 224 has an excited-state oxidation potential (\* $E^{ox}$ ) of -2.24 V, making it a powerful photoreductant. In subsequent work, the same group disclosed a new series of homoleptic W(0) complexes containing oligoarylisocyanide ligands by functionalizing the para position of CNDipp ligand. 169 Through this structural modification, four new W(0) complexes having oligoarylisocyanide ligands were described (225-228). All of these W(0) complexes have excited-state oxidation potentials more negative than -2.29 V, again suggesting they are strong photoreductants. Gray's group further examined the effects of extension of the  $\pi$ -conjugation system of the isocyanide ligands by incorporating alkynyl-aryl units at the para position and using arylisocyanides with fused polycyclic aromatic groups (229-234). Introduction of fused-ring or alkynyl-bridged aryl substituents induces a cathodic shift of the ground-state oxidation potential (E<sup>ox</sup>) by about 300 mV compared to the previous W(0) complexes, but  $E_{0,0}$  values span a small range (~0.15 eV), resulting in a slight decrease in the excited-state reducing power. However, the excited-state potentials of 229-234 (-1.73--2.03 V) are still comparable to or more negative than fac-Ir(ppy)<sub>3</sub>.

Wenger and coworkers demonstrated highly reducing excited states of Mo(0) and Cr(0) complexes having chelating isocyanide ligands (235–237).  $^{171-173}$  Using chelating ligands, the stability of the Mo(0) and Cr(0) complexes is increased relative to monodentate analogues. The excited-state oxidation potentials are  $-2.2\,\mathrm{V}$  for 235,  $-2.3\,\mathrm{V}$  for 236, and  $-2.2\,\mathrm{V}$  for 237. Compound 235 shows photoredox activity in a rearrangement of an acyl cyclopropane to a 2,3-dihydrofuran,  $^{171}$  and 236 outperformed fac-Ir(ppy) $_3$  in a photocatalytic intramolecular base-promoted homolytic aromatic substitution reaction  $^{173}$  due to their strong excited-state reducing ability.

Cerium complexes with electron-rich nitrogen donor ligands, mainly researched by Schelter's group,  $^{174-178}$  are another class of metal complexes with standout excited-state redox properties. In 2016, Schelter and coworkers prepared a mixed-ligand series of Ce(III) complexes (238–241) using  $N,N^\prime$ -diisopropylcarbodiimide (guanidinate) and bis-(trimethylsilyl)amide ligands in different combinations. The UV–Vis absorption peak for all of these compounds is at ca. 420 nm, assigned to a 4f  $\rightarrow$  5d transition, and these compounds can be exceptionally strong photoreductants. As the number of guanidinate ligands increases (moving from 238 to 241), the excited-state oxidation potentials become more negative (–1.63 V for 238, –1.84 V for 239, –2.13 V for 240, and –2.46 V for 241). They demonstrated that

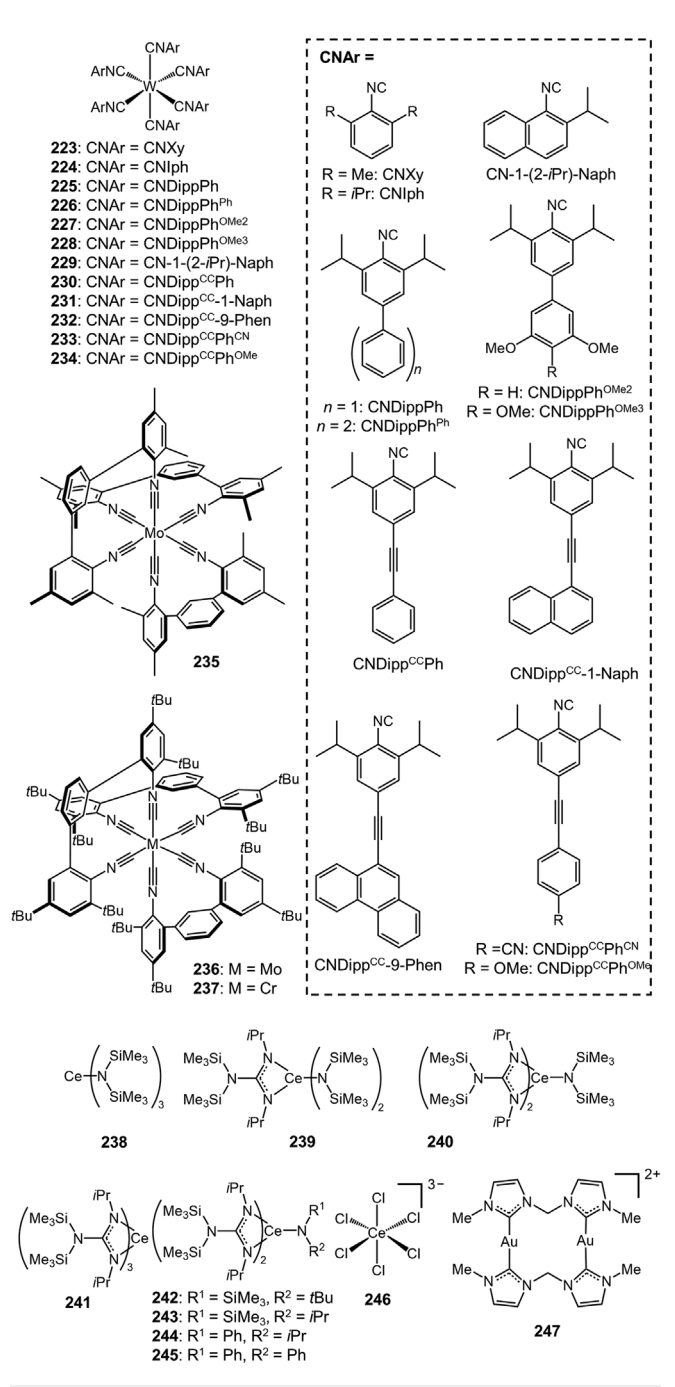


FIG. 12. A series of group 6, Ce(III), and Au(I) complexes.

241 can perform catalytic photoinduced phenylation of 4-fluorophenyl iodide through an outer-sphere electron transfer pathway. Schelter and coworkers then presented a series of Ce(III) complexes (242–245), which have two guanidinate ligands and one amide ligand, modulating the bulkiness of the amide ligand to control structural, electrochemical, photophysical, and photochemical properties of

the Ce(III) complexes.<sup>176</sup> The excited-state oxidation potentials were calculated to be -2.14, -2.14, -2.44, and -2.44 V for **242**, **243**, **244**, and **245**, respectively, showing the trend that complexes with less bulky amide ligand have more reducing potentials. Due to the stronger excited-state reducing power, the yield of the phenylation of 4-bromofluorobenzene increased from 0% using **240** to 66% using **245**. Schelter's group discovered a simple Ce(III) chloride complex, [CeCl<sub>6</sub>]<sup>3-</sup> (**246**), which can be readily prepared *in situ* from CeCl<sub>3</sub> and NEt<sub>4</sub>Cl in acetonitrile solutions.<sup>177,178</sup> The excited-state oxidation potential of **246** is estimated to be  $-3.05\,\text{V}$  ( $-3.45\,\text{V}$  vs Fc<sup>+/0</sup>), although the compound only absorbs UV light. They examined photo-induced reductive dehalogenation of aryl halide substrate using **246** as a photoreductant.<sup>177</sup> The potent excited-state reducing property of **246** enabled the dehalogenation reaction with good yields. In 2018, they also demonstrated the photocatalytic activity of **246** in photoin-duced Miyaura borylation of aryl chlorides and aryl bromides.<sup>178</sup>

Scaiano, Barriault, and coworkers synthesized polynuclear Au(I) complexes with bisphosphine and N-heterocyclic carbene ligands in 2016.<sup>179</sup> These colorless complexes require UVA excitation but are nonetheless strong photoreductants active in photoredox catalytic transformations. Among these Au(I) complexes, a complex supported by the *N*-heterocyclic carbene ligand bis(*N*-methylimidazol-2-ylidene)methane (247) exhibits an excited-state oxidation potential of –2.10 V and shows photocatalytic activity in the reduction of unactivated carbon–halogen bonds.

Whereas most of the above-mentioned photosensitizers based on coordination complexes have been developed as photoreductants, rhenium tricarbonyl complexes are a class of coordination compounds, which have been predominantly developed as photooxidants. These compounds, summarized in Fig. 13, have the general fac- $[Re(CO)_3(L)(N^N)]^{n+}$ , where N^N is a chelating diimine ligand from the 2,2'-bipyridine (bpy) or 1,10-phenanthroline (phen) family, and L is either an anionic or neutral monodentate ligand, giving chargeneutral or cationic complexes, respectively. A thorough review article catalogues the properties of many compounds from this family.<sup>1</sup> Early work on the complex fac-[Re(Cl)(CO)<sub>3</sub>(phen)] (248) established that it is a strong photooxidant, with a  $*E^{\text{red}}$  value of ca. 1.0 V vs SCE. 181 Similarly, Connick et al. demonstrated that the compound fac-[Re(CO)<sub>3</sub>(im)(phen)]<sup>+</sup> (249, im = imidazole) is a strong photooxidant (\* $E^{\text{red}} = 1.2 \text{ V}$ ) capable of oxidizing Cu<sup>+</sup> to Cu<sup>2+</sup> in azurin. <sup>182</sup> This work sets the stage for numerous studies using rhenium tricarbonyl complexes appended to coordinating protein residues to trigger light-driven oxidation of protein cofactors or redox-active amino acids. 183,184 In addition, several dyads featuring rhenium tricarbonyl units have been prepared to model intramolecular photooxidation of tyrosine amino acids. 185,186 The \*E<sup>red</sup> values of one such series were likewise reported to be ca. 1.2 V vs SCE, <sup>185</sup> again signifying the strong excited-state oxidizing character of these complexes and enabling photoinitiated phenol oxidation.

The preceding discussion has focused on specific examples of compounds that were designed and optimized to be strong photoreductants or photooxidants. In many cases, adding substituents to or altering the  $\pi$ -conjugation of conjugated organic molecules or ligands controls the frontier orbital energy levels and optimizes photocatalytic properties. Figure 14 presents an oversimplified description of these effects. Figure 14 shows individually the effects on HOMO and LUMO energy and how they relate to the excited-state reducing or

FIG. 13. Structures of rhenium tricarbonyl photooxidants

oxidizing power, though in reality it is rarely possible to control the HOMO or LUMO independently. In addition, Fig. 14 assumes that the  $E_{0,0}$  value is controlled entirely by the HOMO-LUMO gap, which is not generally true and is an especially gross simplification in triplet photosensitizers. Nevertheless, Fig. 14 can still illustrate general trends that are relevant to designing photosensitizers with extreme redox potentials. When electron-withdrawing groups are introduced or  $\pi$ -conjugation is extended, the HOMO and/or LUMO energy levels are stabilized, as shown in Figs. 14(a) and 14(b). If the LUMO is stabilized [Fig. 14(a)],  $E_{0.0}$  decreases, resulting in a less negative excited state oxidation potential (\*Eox) and weaker reducing power of the excited state. However, the same modifications stabilize the HOMO energy level [Fig. 14(b)], which on its own results in a more positive excited-state reduction potential ( ${}^*E^{\text{red}}$ ), increasing the oxidizing power of the excited-state. On the other hand, introducing electron-donating groups tends to destabilize HOMO and/or LUMO energy levels [Figs. 14(c) and 14(d)]. As depicted in Fig. 14(c), destabilization of the LUMO would increase the HOMO-LUMO gap and  $E_{0.0}$ . This perturbation leads to a more negative oxidation potential of the excited-state (\* $E^{\text{ox}}$ ), making the photosensitizer a stronger photoreductant. If the HOMO level destabilized [Fig. 14(d)],  $E_{0,0}$  is decreased, resulting in a less positive excited-state reduction potential (\*E<sup>red</sup>). Photosensitizers with the less positive \*E<sup>red</sup> value have weaker oxidizing power in the excited state. Again, the reality is that the HOMO and LUMO are usually both perturbed by adding substituents or altering conjugation, so which of the above effects on  $E_{0,0}$ and excited-state potential is observed depends on which frontier orbital is more strongly influenced by the chemical modification.

Another possible scenario is that  $E_{0,0}$  does not change significantly even as the HOMO and LUMO energy level are perturbed, in which case  $^*E^{\rm red}$  and  $^*E^{\rm ox}$  typically shift in the same direction as one another. For example, if the HOMO is stabilized [Fig. 14(b)] without a perturbing  $E_{0,0}$ , both  $^*E^{\rm red}$  and  $^*E^{\rm ox}$  have more positive value (less negative, in terms of  $^*E^{\rm ox}$ ). In that case, the photosensitizer can be a stronger photooxidant as mentioned above, while becoming a weaker photoreductant at the same time.

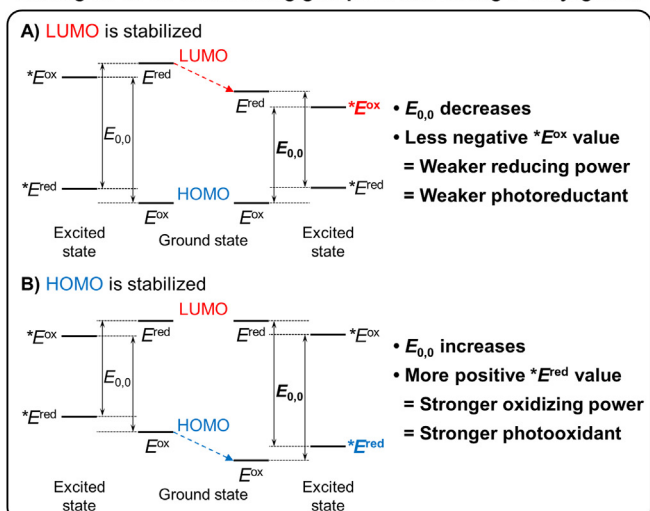
#### B. Two-photon activation

In photoredox catalysis applications, visible-light excitation of the photosensitizer is usually preferred over UV, because many organic substrates and reagents absorb UV light, which can sometimes result in deleterious decomposition pathways. However, the relatively low energy of visible light is thermodynamically insufficient to initiate organic reactions that require high potentials, a limitation that must be overcome to develop methods for more challenging substrates with high redox potentials. One solution developed recently is to use multiphoton excitation methods that combine the energy of two or more photons in one catalytic turnover. 187 The methods described in this review all involve exactly two photons, and there are two major motifs for two-photon activation. Most examples involve two sequential onephoton absorption processes, which combine to generate a powerful photoreductant or photooxidant. This pathway, also termed lightinduced consecutive photoelectron transfer, is described here in Sec. III B 1. The simplified mechanistic pathway of this two-photon activation strategy is illustrated in Fig. 15. Although in principle this strategy can produce strong photooxidants or photoreductants, all the examples in this section involve the latter.

Upon absorption of the first photon  $(h\nu_1)$ , the photosensitizer (PS) enters its excited state (\*PS), which undergoes reductive quenching with a sacrificial electron donor (D) to produce the stable radical anion PS\*-. The excitation of PS\*- by the second photon  $(h\nu_2)$  generates the excited-state radical anion \*PS\*-, which is a potent reductant. Then, \*PS\*- is oxidatively quenched by the substrate to regenerate the neutral ground state of photosensitizer (PS). The other mechanism described at the end of this section involves direct two-photon activation of the photosensitizer, which produces unbound, solvated electrons that serve as the reducing equivalents. The approach outlined in Fig. 15 is desirable for synthetic applications since it can be carried out with conventional LED light sources. Direct two-photon activation requires high-powered laser light sources, less commonly available to synthetic chemists.

Two-photon activations were initially examined by Goez's group in photoionization of  $[Ru(bpy)_3]^{2+}$  for photochemical water

#### Adding electron-withdrawing groups or increasing $\pi$ -conjugation



#### Adding electron-donating groups

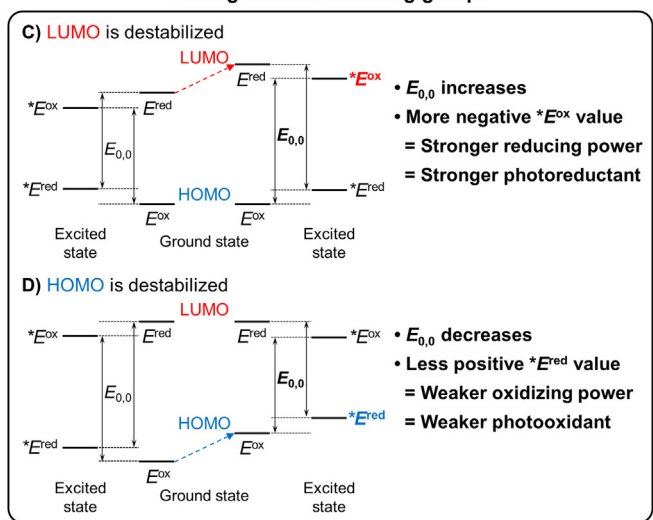


**FIG. 14.** Possible four scenarios controlling ground- and excited-state redox potentials and reducing or oxidizing power of the excited state.

splitting. <sup>188,189</sup> In the context of organic photoredox catalysis, König and coworkers demonstrated reduction and C–H aromatic substitution of aryl halides via two-photon activation of a perylene diimide (PDI, 250). <sup>190</sup> As depicted in Fig. 16, the excited-state \*250 generated by the first photon is reductively quenched by the triethylamine (Et<sub>3</sub>N) sacrificial electron donor. The ground-state radical anion 250° is excited by the second photon to give excited-state radical anion \*250°, which is estimated to have a strong reducing power with a potential that reaches or exceeds the reduction potential of substituted aryl chlorides.

Using these photochemical properties of PDI, researchers have incorporated PDI into metal-organic frameworks (MOFs) and examined photocatalytic activity in photoreduction of aryl halides, <sup>191,192</sup> photooxidation of benzyl alcohols, <sup>191</sup> oxidative coupling of amines

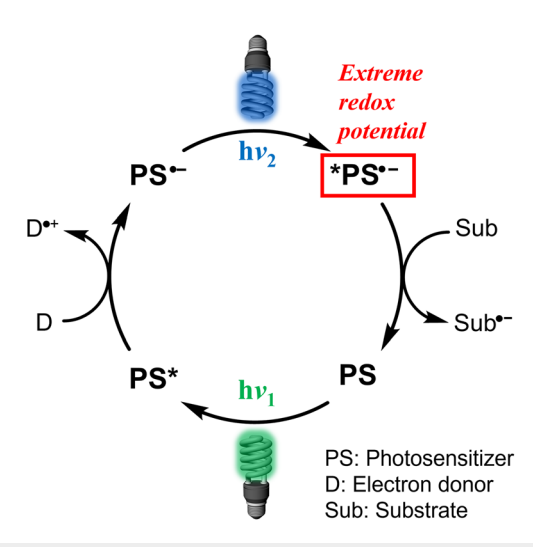


FIG. 15. Two-photon activation strategy.

into imines, <sup>193</sup> oxidation of styrene, <sup>193</sup> and catalytic coupling of epoxides. <sup>192</sup>

König and coworkers selected Rhodamine 6G (Rh-6 $G^+$ , 251 $^+$ ), which is a widely used organic dye in photochemistry as their next target for this two-photon strategy. <sup>194–196</sup> In 2016, they demonstrated the activation of aryl bromide substrates using Rh-6 $G^+$  under irradiation with 530 nm green light and 450 nm blue light. <sup>194</sup> Wavelength-dependent two-photon activation of 251 $^+$  is possible because it absorbs both green and blue light, but the radical 251 $^{\circ}$  only absorbs in the blue region. In the photocatalytic mechanisms they proposed, both the ground-state radical 251 $^{\circ}$  and the excited-state \*251 $^{\circ}$  are active redox species (Fig. 17). Through the sequential activation of aryl bromide substrates by 251 $^{\circ}$  with relatively mild potential [ $E^{\rm red}$ (251 $^{+}$ ) = -1.0 V] and \*251 $^{\circ}$  with highly reducing potential [\* $E^{\rm red}$ (251 $^{\circ}$ ) = -2.4 V], C–C coupling products were synthesized.

In 2017, König and coworkers exhibited photocatalytic methods for one-electron reduction of chlorobenzene using lanthanide-coupled Rh-6G<sup>+</sup>. Some lanthanide(II) salts have negative enough potentials to reduce aryl chlorides, but stoichiometric amounts are needed. They utilized consecutive photoinduced electron transfer strategy to generate lanthanide (II) salts catalytically. As shown in Fig. 18, lanthanidecoupled Rh-6G<sup>+</sup> complex 252 is excited by the first photon and reduced by the DIPEA sacrificial electron donor to yield the reduced radical 252°. The role of the coordinated lanthanide ion is to preclude the back electron transfer to the DIPEA (*N*,*N*-diisopropylethylamine) radical cation in this step. The excited-state radical \*252\* generated by the second photon has significantly higher reducing power. Ln<sup>3+</sup> is reduced by \*252° to Ln<sup>2+</sup>, which transfers an electron to the aryl chloride substrate and then recombines with Rh-6G<sup>+</sup> (251<sup>+</sup>) to be regenerated to 252. Using this cooperative action of Rh-6G<sup>+</sup> and lanthanide ions, they demonstrated C-C and C-P bond formation reactions of aryl radicals produced from aryl chloride substrates.

König's group also reported the use of anthraquinone (Aq) and its derivatives as photocatalysts in dehalogenation of aryl halides and C–C bond forming reactions (Fig. 19). <sup>197</sup> Upon the absorption of the first photon, 1,8-dihydroxyanthraquinone, Aq-OH (253, Fig. 19) is

FIG. 16. Two-photon activation of PDI (250)

excited to \*253, followed by the reductive quenching by TEA. Interestingly, the radical anion Aq-OH\* (253\*) forms semi-quinone anion Aq-OH-H (254) through protonation and successive reduction. Both 253\* and 254 were excited by a second photon and can transfer a single electron to aryl halide substrates to yield aryl radicals, which react in dehalogenation and C–C bond formation reactions.

Pérez-Ruiz and coworkers investigated 9,10-dicyanoanthracene (DCA, 47), <sup>198,199</sup> which is a simple but widely used organic photocatalyst as described in Sec. III A (see Fig. 7). The mechanistic pathway they proposed is that excitation of 47 with blue light leads to the excited-state \*47, which is reductively quenched by DIPEA to form radical anion 47\* Excitation of 47\* under irradiation of green light induces the formation of excited-state \*47\*, which is a highly reducing species. They examined phosphorylation, sulfide formation, and borylation of aryl halide substrates (Fig. 20, substrate class A), demonstrating the capability of 47\* to cleave unactivated C-halide bonds. <sup>198</sup>

In 2021, the same group expanded the substrate scope by reporting activation of five-membered ring heteroarene halides (Fig. 20, substrate class B). <sup>199</sup> Intriguingly, when photocatalyzed phosphorylation of heteroarenes was carried out in a gel-based media, the yield, selectivity, and reaction rate were significantly enhanced, especially for the formation of heteroarene phosphonates. They postulated that the

efficient compartmentalization caused by the gel network induces localization of reactants in the solvent pools between fibers and wide-spread through the fibers, providing a confined but dynamic space for enhanced photochemical reactivity.

In 2018, Sikes and coworkers proposed a mechanism for alkaline, aqueous photoredox catalysis using Eosin Y (256<sup>2-</sup>), triethanolamine (TEOA), and oxygen under green and violet light (Fig. 21). According to their proposed mechanism, 256<sup>2-</sup> is photoreduced by TEOA under irradiation by green light, with the excited-state \*256<sup>2-</sup> undergoing electron transfer to form the radical trianion 256\*<sup>3-</sup>. Excitation of 256\*<sup>3-</sup> by violet light produces the excited radical trianion \*256\*<sup>3-</sup>, which is expected to have faster photoinduced electron transfer rate than the ground-state 256\*<sup>3-</sup>. Since their work mainly focused on controlling the kinetics of elementary steps to introduce a set of tools to favor photocatalyst regeneration, it does specifically comment on the redox potential or redox reactivity of \*256\*<sup>3-</sup>. However, this work does suggest a strategy of using sequential photoinduced electron transfer to favor catalyst regeneration, which is an important step in any catalytic cycle.

The excited-state dynamics of acridinium salts, another widely used organic photocatalyst class (see Fig. 6), were described by Nicewicz's group in 2020. Based on spectroscopic, chemical, and computational studies, they suggested a mechanism depicted in Fig. 22

FIG. 17. Two-photon activation of Rh-6G<sup>+</sup> (251<sup>+</sup>).

for photocatalytic reactions involving aryl halide substrates. Upon irradiation at 390 nm, excitation of 2<sup>+</sup> produces the excited state \*2<sup>+</sup>. Excited-state \*2<sup>+</sup> undergoes reductive quenching with DIPEA, generating 2<sup>\*</sup> and the corresponding DIPEA radical cation. After absorption of the second photon (also 390 nm), 2<sup>\*</sup> is then excited to produce \*2<sup>\*</sup>, assigned as a long-lived twisted intramolecular charge-transfer (TICT) state. The estimated maximum excited-state oxidation potential

following this second excitation,  $^*E^{\rm ox}(2^{\bullet})$ , is  $-3.36\,\rm V$ , suggesting that  $2^{\bullet}$  is an exceptionally strong photoreductant. Photogenerated intermediate  $^*2^{\bullet}$  can engage in electron transfer with aryl halides, producing arene radical anions and regenerating  $2^{+}$ . With this highly reducing photoredox catalyst, they demonstrated reductive dehalogenation of aryl bromides, aryl chlorides, and polyhalogenated aromatics, and identified the reductive detosylation of amine substrates. One

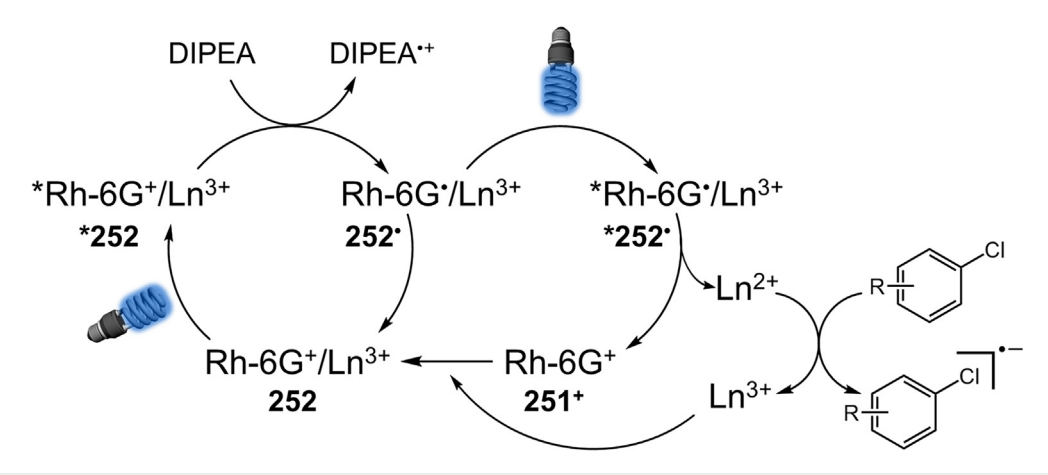
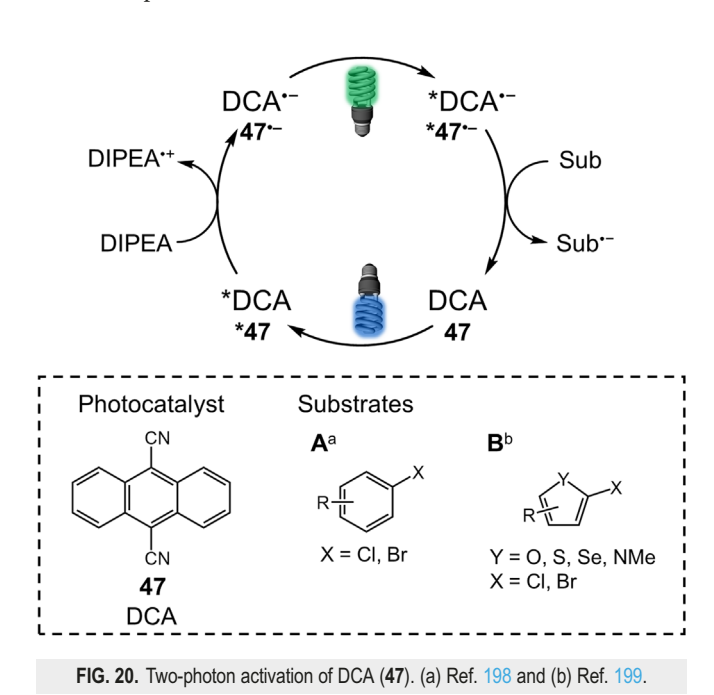


FIG. 18. Lanthanide coupled Rh-6G (252).

FIG. 19. Photocatalytic cycle of anthraquinone (253) via two-photon activation strategy.

significant aspect of this work is that acridinium compounds are normally strong excited-state oxidants under typical one-photon activation (see Fig. 6 and accompanying discussion). However, using the sequential two-photon photoinduced electron transfer described in Fig. 22, it is possible to generate a powerful photoreductant from an acridinium precursor.

Researchers have presented two-photon activation strategies using metal-based photocatalysts as well. König and coworkers demonstrated photocatalytic activation of stable, water insoluble, lipophilic alkyl chloride substrates using [Ir(ppy)<sub>2</sub>(dtbpy)]<sup>+</sup> (257<sup>+</sup>) with an



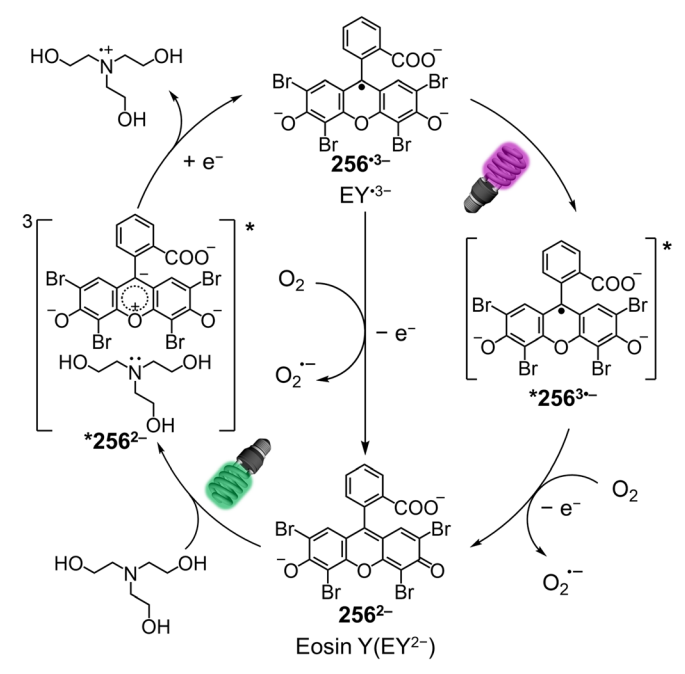


FIG. 21. Two-photon activation of Eosin Y (256<sup>2-</sup>)

**FIG. 22.** Photocatalytic cycle of Mes-Acr (2<sup>+</sup>) via two-photon activation.

assembly promoted single electron transfer strategy.<sup>201</sup> They used the mixture of sodium lauryl oligoethylene glycol sulfate (SLES) and water to produce a microstructured solution system within and around a micelle formed by SLES. In this structural design, the reactive species can be compartmentalized in a microstructured heterogeneous aqueous solution as illustrated in Fig. 23. These micelles provide solubilization of water-insoluble alkyl chlorides and allow hydrophilic chlorine atoms to point toward the surface of the micelles, leading to proximity to 257<sup>+</sup>, which is noncovalently immobilized on the negatively charged micelle surface. Upon successive irradiation by blue light and reductive quenching by ascorbate, 257<sup>+</sup> is transformed to the radical 257°. The excited-state \*257° is formed by the consecutive excitation with a second photon, and this excited state is reducing enough to transfer an electron to alkyl chloride substrates generating the alkyl chloride radical anion. Due to the high hydration energy of chloride anion in aqueous media, the C-Cl bond is cleaved to produce an alkyl radical that can form the dehalogenation product or participate in C-C coupling reactions.

In 2019, Connell and coworkers reported a tandem photocatalytic mechanism comprising two inter-connected photoredox cycles as shown in Fig. 24.<sup>202</sup> In the mechanism they proposed, radical 257\*, which is formed by blue light irradiation [step (i)] and reductive quenching by TEA [step (ii)], can react with readily reducible substrates to complete the photoredox cycle [step (iii)], regenerating 257<sup>+</sup> [ $E^{\text{red}}(257^+) = -1.47 \text{ V}$ ]. A second possible fate for 257\* is conversion to a new semi-hydrogenated complex 258 via hydrogen atom transfer [step (iv)]. Absorption of the second photon [step (v)] by 258

produces an excited state, which is a significantly stronger reductant  $[*E^{ox}(258) = -1.7 \, V]$ . Excited-state \*258 can reduce aryl and alkyl halide substrates though electron transfer (ET) or proton-coupled electron transfer (PCET) processes [step (vi)]. The oxidized form of 258, 258 $^+$ , can readily react with 257 $^+$  to regenerate 258 and 257 $^+$ , closing the photocatalytic cycle [step (vii)]. The authors also considered a possibility of hydrogen atom transfer from the oxidized 258 $^+$  to re-form 257 [step (viii)]. Recently, some of the same authors applied this tandem photoredox catalysis to the reductive activation and hydrofunctionalization of olefins.  $^{203}$ 

The second major mechanism for two-photon activation involves photoionization of the sensitizer in water to generate solvated electrons  $(e_{aq}^{\bullet -})$ . This approach is perhaps less generalizable than the previously described sequential approach. Photoionization with visible light normally involves excitation or photoreduction with the first photon to generate a relatively short-lived and unstable species, which is then ionized with a second photon. As a result, high-powered laser excitation sources are needed since conventional light sources do not have enough photon flux to ionize the unstable intermediate prior to decomposition. Goez's group has thoroughly studied the photoionization of  $[Ru(bpy)_3]^{2+}$  (123<sup>2+</sup>) to form hydrated electrons, which when generated during a photocatalytic cycle have potent reducing power. 188,189,204-212 As depicted in Fig. 25, irradiation with the first photon in the presence of a sacrificial electron donor produces radical species 123°+. This one-electron-reduced form, which contains a localized bipyridine radical anion, is stable for seconds in deaerated aqueous solution. 213 Upon irradiation with the second photon, 123°+

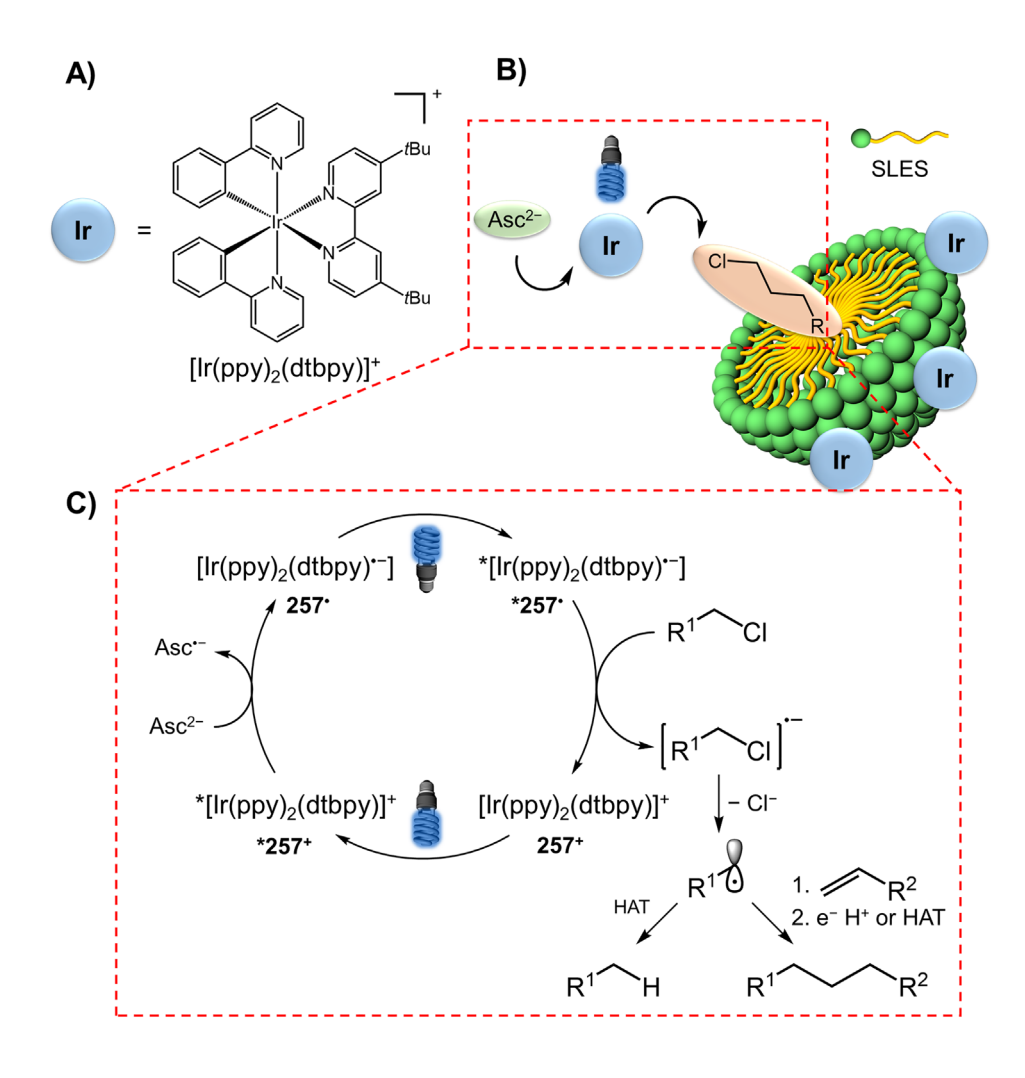


**FIG. 23.** (a) Structure of [Ir(ppy)<sub>2</sub>(dtbpy)]<sup>+</sup> (257<sup>+</sup>). (b) Schematic representation of microstructured solution system. (c) Two-photon activation of 257<sup>+</sup>.

expels a hydrated electron,  $e_{aq}$ . With this photocatalytic cycle, they demonstrated the applicability of  $e_{aq}$  in many difficult reactions.  $^{207-212}$ 

In 2019, Wenger and coworkers also produced hydrated electron through a two-photon mechanism using a water-soluble Ir complex 138<sup>3-</sup> in the presence of TEOA as sacrificial electron donor and blue region light source. <sup>142</sup> Their proposed mechanism, also shown in Fig. 25, is slightly different. Excitation of complex 138<sup>3-</sup> initially produces the <sup>3</sup>MLCT excited state (\*138<sup>3-</sup>), which is intercepted by the second photon and ionized to form the oxidized 138<sup>3-</sup> and the solvated electron. Capture of 138<sup>2-</sup> with the sacrificial donor closes the photocycle. This strongly reducing photosystem was demonstrated to be capable of a few challenging dehalogenation reactions and can degrade the benzyltrimethylammonium cation.

#### C. Combined photo- and electro-chemical activations

In the field of synthetic organic redox chemistry, the selective activation of challenging substrates with high redox potentials (i.e., very positive or very negative) is imperative to design and functionalize target molecules and develop synthetic methods with broad substrate scopes. In recent decades, synthetic chemists have used concepts from

photochemistry<sup>214–218</sup> and electrochemistry<sup>219–223</sup> to drive method development. There is some conceptual overlap between photochemical and electrochemical catalytic methods, which share the common feature of typically involving radical intermediates generated through single electron transfer (SET) processes. However, each method has innate drawbacks and limits in terms of efficiency, cost, or environmental issues that impede promising results in much more challenging reactions. In photoredox catalytic systems, the photosensitizer radical cation/anion, produced by reductive or oxidative quenching, must be restored to the closed-shell species, which often requires a stoichiometric amount of a sacrificial reductant or oxidant. These additives can provide unwanted reaction pathways and generate stoichiometric byproducts. As discussed above, in the case of visible-light photocatalysis, the energy of visible-light sources is insufficient for the activation of challenging organic substrates, such as reduction of aryl chlorides<sup>224</sup> and silyl chlorides,  $^{225}$  which require at least  $-2.6\,\mathrm{V}$  of potential. The critical limitation of electrochemical methods is a high ohmic drop due to the low conductivity of organic solvents. This often necessitates the use of a supporting electrolyte, which can hamper product separation, or can be overcome by applying higher potential to the reaction,

**FIG. 24.** Tandem photocatalytic mechanism of **257**<sup>+</sup>.

which can induce unwanted and deleterious redox processes that erode selectivity. <sup>226,227</sup>

The merger of photochemical and electrochemical methods allows synergism of their advantages, making possible straightforward access to novel reactions that are difficult or impossible with either method on its own. The concept of combined photo- and electrochemical methods in terms of organic synthesis was first suggested by Moutet and Reverdy with their work on photoexcited electrochemically generated radical ion. After that, Rusling and coworkers studied photoexcitation of electrochemically generated anthracene radical anion. The radical anion successfully reduced 4-chlorobiphenyl under irradiation by visible light. However, further studies had not been carried out until recently despite these fascinating early conceptual advances.

Photoelectrochemistry, which is the combination of a photocatalytic system with an electrochemical cell, can be categorized by a few distinct mechanistic pathways as illustrated in Fig. 26.<sup>230,231</sup> (Researchers often use their own terminology, but the IUPAC recommends the use of the term "photoelectrochemistry" for "a field of chemistry employing techniques which combined photochemical and electrochemical methods for the study of the oxidation–reduction chemistry of the ground or excited states of molecules or ions."<sup>232</sup> So, we use the term photoelectrochemistry here.) In the traditional concept, the photoelectrocatalytic system [Fig. 26(a)] is composed of a single electrochemical cell with a photoanode coated in photoresponsive

materials such as semiconductors or metal complexes.<sup>5,233–239</sup> In decoupled photoelectro-chemistry [Fig. 26(b)], two distinct photoexcitation and electrochemical process activate two discrete chemical species.<sup>2,40–2,42</sup>

Unlike the aforementioned two cases, in photoelectrochemistry processes applied to organic synthesis [Figs. 26(c) and 26(d)], pioneered in large part by Lambert's and Xu's groups, 243-252 the photoexcitation and electrochemistry steps occur in tandem to activate a single chemical species, which is normally a photocatalyst. These two figures depict reactions that involve substrate oxidation, in which the electrochemical reaction of the photosensitizer occurs at the anode, but it is also possible to carry out reductive transformations in which the key electrochemical step is cathodic. In the chemical oxidant-free system [Fig. 26(c)], an electrochemical reaction restores the photosensitizer by reducing or oxidizing the radical ion formed by excited-state quench-In this part, we want to focus on the photoexcitation of electrochemically generated radical ions as depicted in Fig. 26(d). These excited-state radical ions of the photosensitizer can exhibit extreme redox potentials. This approach can be used to either generate strong photooxidants, normally by oxidation of the photosensitizer [as shown in Fig. 26(d)], or strong photoreductants by initial reduction of the photosensitizer.

In 2019, Lambert's and coworkers demonstrated the possibility of triamino-cyclopropenium (TAC) ion as a potent oxidative

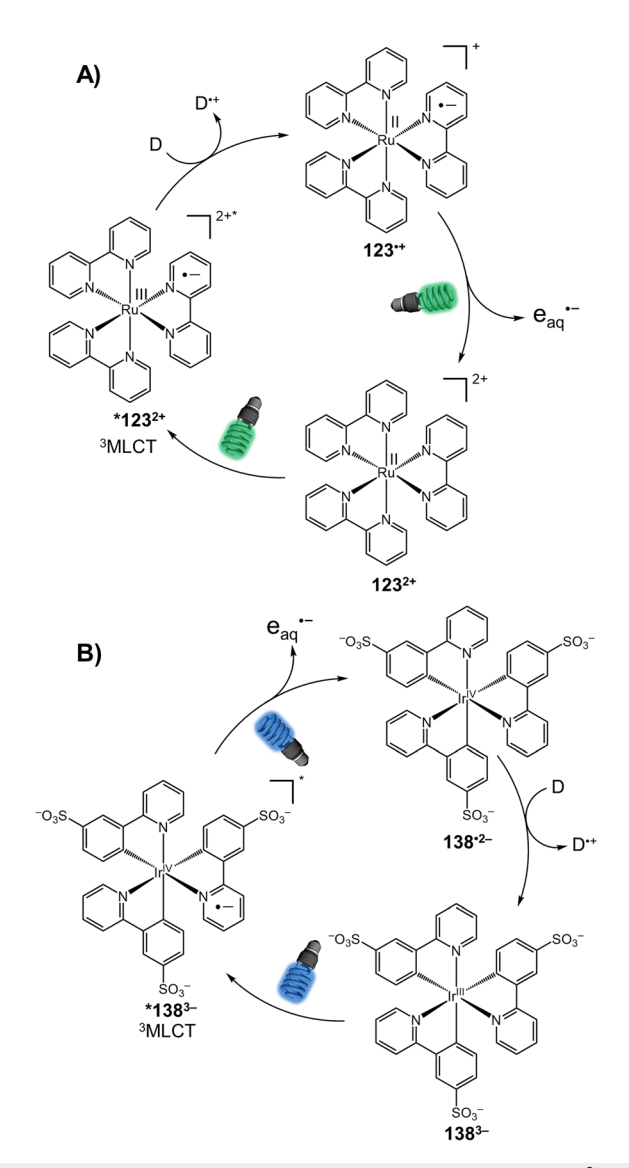


FIG. 25. Generation of hydrated electrons via two-photon activation of  $123^{2+}$  (a) and  $138^{3-}$  (b).

electrophotocatalyst.<sup>248</sup> They demonstrated that the TAC ion (259<sup>+</sup>) is electrochemically oxidized to form a radical dication intermediate, 259<sup>+2+</sup>. This dication is an extremely strong photooxidant (\*E<sup>red</sup> = 3.33 V), so photoexcitation of this electrochemical intermediate produces excited-state species (\*259<sup>+2+</sup>), which can oxidize the substrate (Fig. 27). With this highly oxidizing photoexcited radical dication, they examined many challenging organic reactions such as the oxidative coupling of benzene and pyrazole, <sup>248</sup> C-H functionalization of ethers, <sup>249</sup> C-H amination via Ritter-type reaction, <sup>247</sup> acetoxyhydroxylation of aryl olefins, <sup>251</sup> and diamination of vicinal C-H bonds. <sup>252</sup>

In 2020, Lambert, Lin, and coworkers demonstrated that they can generate the highly reducing excited-state radical anion of dicyanoanthracene (DCA) via tandem electrochemical reduction and photoexcitation.<sup>250</sup> As presented in Fig. 28, cathodic reduction of DCA

(47) produces radical anion  $47^{*-}$ . The photoexcitation of  $47^{*-}$  (\* $E^{ox} = -3.2 \,\mathrm{V}$ ) produces the excited-state radical anion \* $47^{*-}$ , which is proposed to undergo SET with the aryl halide substrates. The redox potential of \* $47^{*-}$  is strong enough to activate aryl bromides and aryl chlorides, generating aryl radicals, which were functionalized in different ways.

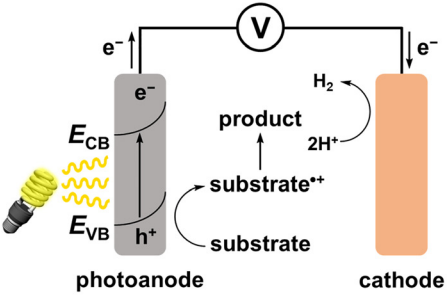
Another example of potent reductants via photoelectrochemical process was described by Wickens and coworkers in 2020 (Fig. 29). They studied the naphthalene-based chromophore NpMI (260). The photoexcitation of electrochemically generated  $260^{\circ}$  provides the excited-state radical anion \* $260^{\circ}$ , which exhibits about -3.3 V reducing potential. Using \* $260^{\circ}$ , they successfully demonstrated the functionalization of aryl chloride substrates having electron-donating groups, which are considered as challenging substrates due to their negative reduction potentials (<-3.0 V).

Although the radical cation/anion photochemistry described in Secs. III B and III C has become a prominent mechanistic dogma in organic synthesis, and thermodynamic analysis of the radical species does indicate they are strong reductants or oxidants, recent spectroscopic and photochemical investigations have questioned the initially proposed mechanistic pathways and the role of photoexcited radical ions in these reactions. Early studies on the PDI radical anion (PDI\*-) revealed that its doublet excited state has a very short lifetime of ca. 160 ps, 256 which on its own calls into question later suggestions of its role in bimolecular redox chemistry. Mechanistic studies by Marchini et al. suggested that a further decomposition product of PDI was the active photoreductant in the work summarized in Fig. 16 above.<sup>2</sup> Relatedly, Zeman et al. showed that PDI\* is quenched by some aryl halides but not others, suggesting it may not always be involved in the dehalogenation reaction, and used Rehm-Weller analysis to suggest that  $^*E^{\text{ox}}$  for PDI $^{\bullet-}$  is  $-1.87\,\text{V}$  vs SCE, much less potent than initially reported.<sup>258</sup> Similar controversies have arisen with the DCA radical anion (47°-), which has a very short excited-state lifetime of 3 ps.

In light of the above controversies, there are two recent studies that put forth alternative mechanistic proposals for radical anion photochemistry. The Nocera group used time-resolved spectroscopic techniques to study the photophysics and photochemistry of the NpMI radical anion  $260^{\bullet-}$ ,  $^{260}$  with key results summarized in Fig. 30. They found that the excited-state lifetime of  $^*260^{\bullet-}$  is 24 ps, too short for bimolecular redox chemistry. However, a second proton-coupled reduction of  $^*260^{\bullet-}$ , which is operative under typical photoredox conditions, generates the Meisenheimer complex 261. Compound 261 is a closed-shell species with a 20-ns singlet excited-state lifetime and an excited-state oxidation potential ( $^*E^{ox}$ ) of -2.68 V, making it a sufficiently strong photoreductant with a long enough lifetime to activate aryl chloride substrates in a bimolecular fashion.

Li and Wenger have recently demonstrated that the closed-shell PDI dianion has a longer excited state lifetime than the radical monoanion PDI species, as illustrated in Fig. 31. Spectroscopic and electrochemical studies of four PDI compounds [Fig. 31(a)] were carried out both in water and in organic solvent. The lifetime of the excited state of radical monoanion (\*PDI\*) is 160 ps, which is too short for diffusion-controlled bimolecular reactions. By contrast, the PDI dianion species, PDI\$^-, which was produced by reaction with sodium dithionite (Na2S2O4), exhibited a longer lifetime of 6.4 ns. Furthermore, the \* $E^{ox}$  value of PDI\$^- was estimated to be -2.7 V, suggesting a strong reducing power.

# A) Photoelectrocatalytic system



### B) Decoupled photoelectrochemistry

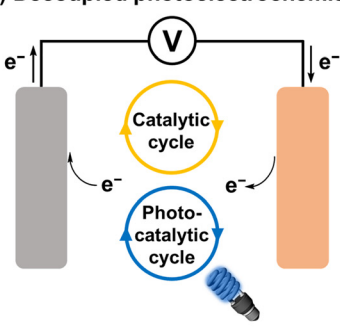
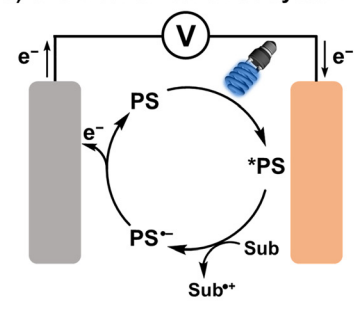
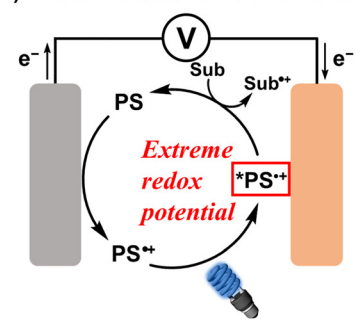


**FIG. 26.** Four categories of photoelectrochemistry.

#### C) Chemical oxidant-free system



#### D) Photoexcitation of radical ions



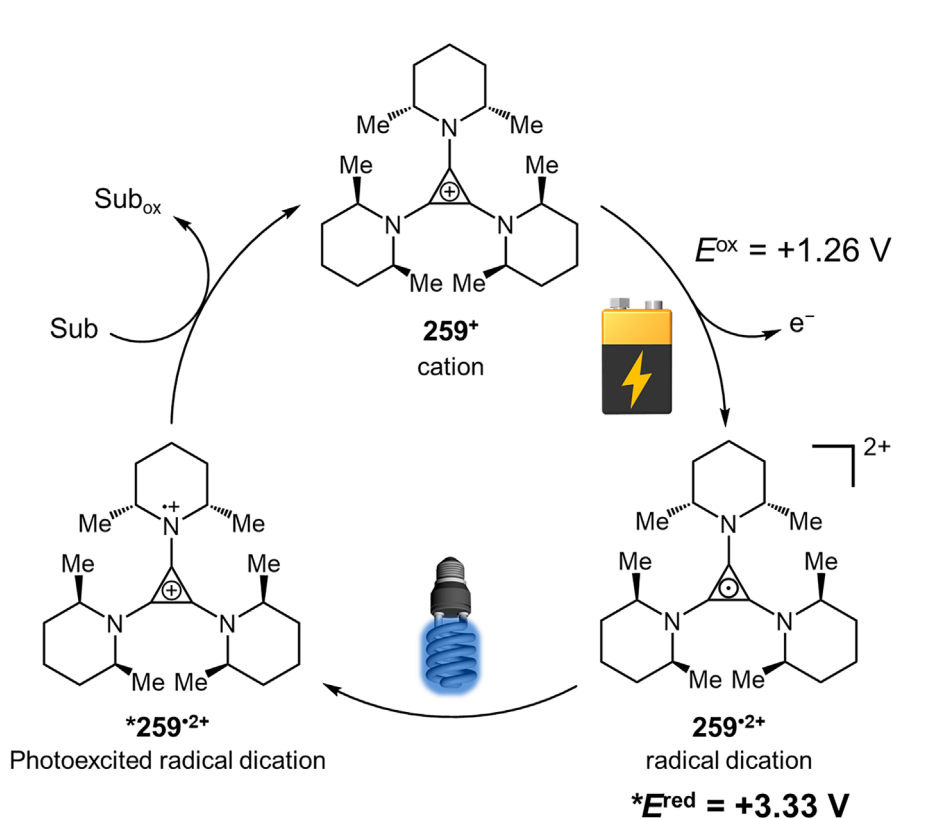


**FIG. 27.** Photoelectrochemical catalytic cycle of TAC (259<sup>+</sup>).

$$E^{\text{red}} = -0.82 \text{ V}$$
 $A7$ 
 $A7$ 

**FIG. 28.** Activation of aryl halides with DCA (**47**) via photoelectrochemistry.

FIG. 29. Potent reducing property of NpMI (260) via photoelectrochemical process.

Ar—N

260°-

$$\tau = 24 \text{ ps}$$

\* $E^{\text{ox}} = -3.3 \text{ V}$ 
 $e^{-}, H^{+}$ 

Ar—N

 $\theta = 0$ 
 $\theta =$ 

**FIG. 30.** Generation of Meisenheimer complex **261**, proposed to be the active photoreductant in NpMI "radical anion" photochemistry.

#### IV. CONCLUSION

In this focused review article, we presented three strategies for accessing photogenerated species with extreme redox potentials. The most conventional and widely applied strategy is via molecular design, producing organic or metal-based photosensitizers that have appropriately positioned frontier orbitals to allow for visible-light generation of powerful reductants or oxidants. There has been a steady outgrowth of conceptual and practical advances over the past 20 years or more that

have allowed many classes of potent photoreductants and photooxidants, many of which are intentionally designed to allow photoredox transformations on challenging substrates. Given the recency of many of these developments, we anticipate continued progress in the discovery of designer photosensitizers well-suited for photoinduced redox chemistry with challenging substrates.

There is no strict theoretical limit on how strong of a photooxidant or photoreductant can be designed using conventional approaches, since the excited-state redox potentials depend both on the ground-state potentials and the excited-state energy. However, given the limited energy of visible photons, there are practical challenges associated with accessing excited-state redox reagents with reducing potentials more negative than  $-2.5 \,\mathrm{V}$  or more oxidizing than +2.0 V. The other two directions covered in this review overcome this limitation, relying on additional energy input to access strong redox reagents via photochemistry, either in the form of two-photon activation or combined electrochemical/photochemical activation. In most cases, these two approaches share the common feature of involving a stable radical cation or anion, accessed via an initial photoredox step or via electrochemistry, which is then excited by visible light to produce an exceptionally strong oxidant or reductant. These approaches have only recently gained popularity in synthetic applications, but in many cases, they do result in redox potentials that are not accessible via conventional one-photon approaches. It remains to be seen how

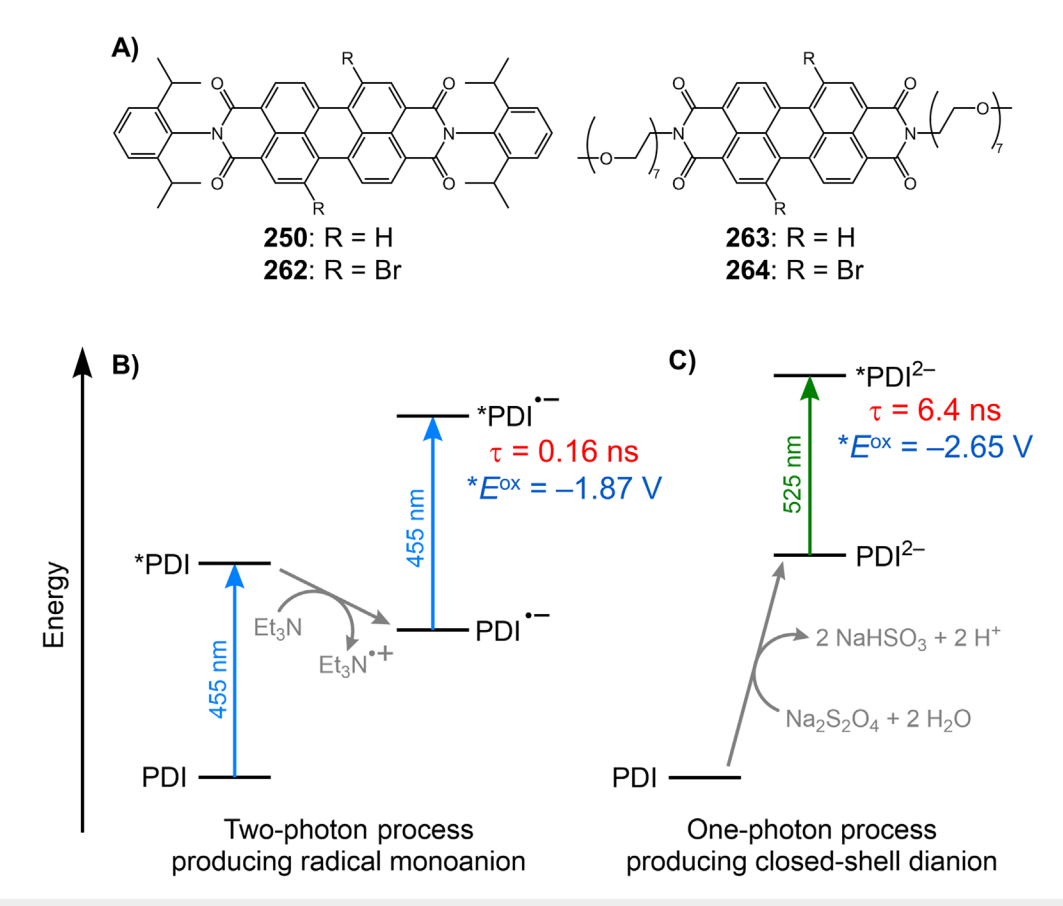


FIG. 31. (a) Molecular structures of PDI compounds. (b) Formation of photoexcited PDI radical monoanion and (c) closed-shell dianion.

generalizable these approaches are, given the inherent technical complexity in executing two-photon excitation or photoelectrochemical activation, but the early developments are certainly promising and foretell many exciting future developments.

#### **ACKNOWLEDGMENTS**

We thank the National Science Foundation (Grant No. CHE-1846831), the Welch Foundation (Grant No. E-1887), and the University of Houston, through the High Priority Area Research Seed Grants, for funding our group's work on photosensitizer design and applications.

#### **AUTHOR DECLARATIONS**

#### Conflict of Interest

The authors have no conflicts to disclose.

#### DATA AVAILABILITY

Data sharing is not applicable to this article as no new data were created or analyzed in this study.

#### REFERENCES

- <sup>1</sup>T. R. Cook, D. K. Dogutan, S. Y. Reece, Y. Surendranath, T. S. Teets, and D. G. Nocera, Chem. Rev. 110, 6474 (2010).
- <sup>2</sup>T. S. Teets and D. G. Nocera, Chem. Commun. 47, 9268 (2011).
- <sup>3</sup>G. Knör, Coord. Chem. Rev. **304–305**, 102 (2015).
- <sup>4</sup>A. Hagfeldt, G. Boschloo, L. Sun, L. Kloo, and H. Pettersson, Chem. Rev. 110, 6595 (2010).
- <sup>5</sup>J.-F. Yin, M. Velayudham, D. Bhattacharya, H.-C. Lin, and K.-L. Lu, Coord. Chem. Rev. 256, 3008 (2012).
- <sup>6</sup>J. Cong, X. Yang, L. Kloo, and L. Sun, Energy Environ. Sci. 5, 9180 (2012).
- <sup>7</sup>M. Schmittel and A. Burghart, Angew. Chem. Int. Ed. Engl. **36**, 2550 (1997).
- <sup>8</sup>C. Dai, J. M. R. Narayanam, and C. R. J. Stephenson, Nat. Chem. 3, 140 (2011).
- <sup>9</sup>D. A. Nagib and D. W. C. MacMillan, Nature **480**, 224 (2011).
- 10 H. Huo, X. Shen, C. Wang, L. Zhang, P. Röse, L.-A. Chen, K. Harms, M. Marsch, G. Hilt, and E. Meggers, Nature 515, 100 (2014).
- <sup>11</sup>C. K. Prier, D. A. Rankic, and D. W. C. MacMillan, Chem. Rev. 113, 5322 (2013).
- <sup>12</sup>K. L. Skubi, T. R. Blum, and T. P. Yoon, Chem. Rev. **116**, 10035 (2016).
- <sup>13</sup>N. A. Romero and D. A. Nicewicz, Chem. Rev. 116, 10075 (2016).
- <sup>14</sup>D. M. Arias-Rotondo and J. K. McCusker, Chem. Soc. Rev. 45, 5803 (2016).
- 15Y. Chi, T.-K. Chang, P. Ganesan, and P. Rajakannu, Coord. Chem. Rev. 346, 91 (2017).
- <sup>16</sup>Y. Lee and M. S. Kwon, Eur. J. Org. Chem. **2020**, 6028.
- <sup>17</sup>M. L. Marin, L. Santos-Juanes, A. Arques, A. M. Amat, and M. A. Miranda, Chem. Rev. 112, 1710 (2012).
- <sup>18</sup>S. Fukuzumi and K. Ohkubo, Org. Biomol. Chem. **12**, 6059 (2014).
- <sup>19</sup>M. V. Bobo, J. J. Kuchta, and A. K. Vannucci, Org. Biomol. Chem. 19, 4816
- <sup>20</sup>J.-H. Shon and T. S. Teets, ACS Energy Lett. **4**, 558 (2019).
- <sup>21</sup>J.-H. Shon and T. S. Teets, Comments Inorg. Chem. **40**, 53 (2020).
- 222 Y. Wu, D. Kim, and T. S. Teets, Synlett (published online 2021).
- <sup>23</sup>R. A. Marcus, J. Chem. Phys. **24**, 966 (1956).
- <sup>24</sup>R. A. Marcus, J. Chem. Phys. **43**, 679 (1965).
- <sup>25</sup>R. A. Marcus, Angew. Chem. Int. Ed. Engl. **32**, 1111 (1993).
- <sup>26</sup>D. Rehm and A. Weller, Isr. J. Chem. **8**, 259 (1970).
- <sup>27</sup>T. Caronna, S. Morrocchi, and B. M. Vittimberga, J. Am. Chem. Soc. 108, 2205 (1986).
- <sup>28</sup>J. C. Croney, M. K. Helms, D. M. Jameson, and R. W. Larsen, Biophys. J. 84, 4135 (2003).
- <sup>29</sup>M. E. McCarroll, Y. Shi, S. Harris, S. Puli, I. Kimaru, R. Xu, L. Wang, and D. J. Dyer, J. Phys. Chem. B 110, 22991 (2006).

- <sup>30</sup>A. (Arman) Taherpour, Arabian J. Chem. **10**, S609 (2017).
- <sup>31</sup>S. E. Braslavsky, Pure Appl. Chem. **79**, 293 (2007).
- 32 The IUPAC Compendium of Chemical Terminology: The Gold Book, 4th ed., edited by V. Gold [International Union of Pure and Applied Chemistry (IUPAC), Research Triangle Park, NC, 2019].
- <sup>33</sup>A. M. Brown, C. E. McCusker, and J. K. McCusker, Dalton Trans. 43, 17635 (2014).
- <sup>34</sup>L. Buzzetti, G. E. M. Crisenza, and P. Melchiorre, Angew. Chem. Int. Ed. 58,
- 35Y. K. Radwan, A. Maity, and T. S. Teets, Inorg. Chem. 54, 7122 (2015).
- <sup>36</sup>J.-H. Shon, S. Sittel, and T. S. Teets, ACS Catal. **9**, 8646 (2019).
- <sup>37</sup>M.-H. Baik and R. A. Friesner, J. Phys. Chem. A **106**, 7407 (2002).
- 38Y. Fu, L. Liu, H.-Z. Yu, Y.-M. Wang, and Q.-X. Guo, J. Am. Chem. Soc. 127, 7227 (2005).
- <sup>39</sup>M. R. Silva-Junior, M. Schreiber, S. P. A. Sauer, and W. Thiel, J. Chem. Phys. 129, 104103 (2008).
- 40 H.-H. G. Tsai, H.-L. S. Sun, and C.-J. Tan, J. Phys. Chem. A 114, 4065 (2010).
- <sup>41</sup>D. Jacquemin, B. Mennucci, and C. Adamo, Phys. Chem. Chem. Phys. 13, 16987 (2011).
- <sup>42</sup>B. Suo, K. Shen, Z. Li, and W. Liu, J. Phys. Chem. A **121**, 3929 (2017).
- <sup>43</sup>E. M. Espinoza, J. A. Clark, J. Soliman, J. B. Derr, M. Morales, and V. I. Vulley, J. Electrochem. Soc. 166, H3175 (2019).
- 44S. Ferrere and B. A. Gregg, J. Am. Chem. Soc. 120, 843 (1998).
- 45 F. Liu and G. J. Meyer, Inorg. Chem. 42, 7351 (2003).
- 46 S. Ardo and G. J. Meyer, Chem. Soc. Rev. 38, 115 (2009).
- <sup>47</sup>G. Li, K. Hu, C. Yi, K. L. Knappenberger, G. J. Meyer, S. I. Gorelsky, and M. Shatruk, J. Phys. Chem. C 117, 17399 (2013).
- <sup>48</sup>J. C. Brauer, A. Marchioro, A. A. Paraecattil, A. A. Oskouei, and J.-E. Moser, . Phys. Chem. C 119, 26266 (2015).
- <sup>49</sup>N. G. Connelly and W. E. Geiger, Chem. Rev. **96**, 877 (1996).
- <sup>50</sup>V. V. Pavlishchuk and A. W. Addison, Inorg. Chim. Acta **298**, 97 (2000).
- <sup>51</sup>M. Hissler, J. E. McGarrah, W. B. Connick, D. K. Geiger, S. D. Cummings, and R. Eisenberg, Coord. Chem. Rev. 208, 115 (2000).
- <sup>52</sup>P. Du, J. Schneider, P. Jarosz, and R. Eisenberg, J. Am. Chem. Soc. 128, 7726
- <sup>53</sup>P. Du, K. Knowles, and R. Eisenberg, J. Am. Chem. Soc. **130**, 12576 (2008).
- <sup>54</sup>F. D'Souza and O. Ito, Coord. Chem. Rev. **249**, 1410 (2005).
- <sup>55</sup>D. M. Guldi, Chem. Soc. Rev. **31**, 22 (2002).
- <sup>56</sup>J. Jiang, J. A. Spies, J. R. Swierk, A. J. Matula, K. P. Regan, N. Romano, B. J. Brennan, R. H. Crabtree, V. S. Batista, C. A. Schmuttenmaer, and G. W. Brudvig, J. Phys. Chem. C 122, 13529 (2018).
- 57S. Fukuzumi, K. Ohkubo, T. Suenobu, K. Kato, M. Fujitsuka, and O. Ito, J. Am. Chem. Soc. 123, 8459 (2001).
- 58S. Fukuzumi, H. Kotani, K. Ohkubo, S. Ogo, N. V. Tkachenko, and H. Lemmetyinen, J. Am. Chem. Soc. 126, 1600 (2004).
- <sup>59</sup>B. Zilate, C. Fischer, and C. Sparr, Chem. Commun. **56**, 1767 (2020).
- 60 A. Tlili and S. Lakhdar, Angew. Chem. Int. Ed. 60, 19526 (2021).
- <sup>61</sup>A. Joshi-Pangu, F. Lévesque, H. G. Roth, S. F. Oliver, L.-C. Campeau, D. Nicewicz, and D. A. DiRocco, J. Org. Chem. **81**, 7244 (2016). <sup>62</sup>A. White, L. Wang, and D. Nicewicz, Synlett **30**, 827 (2019).
- 63 C. Fischer and C. Sparr, Tetrahedron 74, 5486 (2018).
- 64C. Fischer and C. Sparr, Angew. Chem. Int. Ed. 57, 2436 (2018).
- 65C. Fischer, C. Kerzig, B. Zilate, O. S. Wenger, and C. Sparr, ACS Catal. 10, 210 (2020).
- 66 A. Gini, M. Uygur, T. Rigotti, J. Alemán, and O. García Mancheño, Chem. Eur. J. 24, 12509 (2018).
- 67T.-Y. Shang, L.-H. Lu, Z. Cao, Y. Liu, W.-M. He, and B. Yu, Chem. Commun. 55, 5408 (2019).
- <sup>68</sup>P. P. Singh and V. Srivastava, Org. Biomol. Chem. **19**, 313 (2021).
- <sup>69</sup>K. Ohkubo, K. Suga, K. Morikawa, and S. Fukuzumi, J. Am. Chem. Soc. 125,
- 70 Y. Wang, O. Haze, J. P. Dinnocenzo, S. Farid, R. S. Farid, and I. R. Gould, J. Org. Chem. 72, 6970 (2007).
- <sup>71</sup>D. R. Arnold and A. J. Maroulis, J. Am. Chem. Soc. **98**, 5931 (1976).
- 72 J. Luo and J. Zhang, ACS Catal. 6, 873 (2016).
- 73J. Lu, B. Pattengale, Q. Liu, S. Yang, W. Shi, S. Li, J. Huang, and J. Zhang, J. Am. Chem. Soc. 140, 13719 (2018).

- <sup>74</sup>E. Speckmeier, T. G. Fischer, and K. Zeitler, J. Am. Chem. Soc. **140**, 15353 (2018).
- 75 V. Babin, A. Talbot, A. Labiche, G. Destro, A. Del Vecchio, C. S. Elmore, F. Taran, A. Sallustrau, and D. Audisio, ACS Catal. 11, 2968 (2021).
- <sup>76</sup>D. Kong, M. Munch, Q. Qiqige, C. J. C. Cooze, B. H. Rotstein, and R. J. Lundgren, J. Am. Chem. Soc. **143**, 2200 (2021).
- <sup>77</sup>H. Huang, C. Yu, Y. Zhang, Y. Zhang, P. S. Mariano, and W. Wang, J. Am. Chem. Soc. **139**, 9799 (2017).
- <sup>78</sup>Z.-Y. Song, C.-L. Zhang, and S. Ye, Org. Biomol. Chem. **17**, 181 (2019).
- <sup>79</sup>T. C. Sherwood, H.-Y. Xiao, R. G. Bhaskar, E. M. Simmons, S. Zaretsky, M. P. Rauch, R. R. Knowles, and T. G. M. Dhar, J. Org. Chem. **84**, 8360 (2019).
- 80 N. R. Patel, C. B. Kelly, A. P. Siegenfeld, and G. A. Molander, ACS Catal. 7, 1766 (2017).
- 81H. Jiang and A. Studer, Chem. Eur. J. 25, 516–520 (2018).
- 82 T. C. Sherwood, N. Li, A. N. Yazdani, and T. G. M. Dhar, J. Org. Chem. 83, 3000 (2018).
- 83Q.-F. Bao, Y. Xia, M. Li, Y.-Z. Wang, and Y.-M. Liang, Org. Lett. 22, 7757 (2020).
- 84F. Le Vaillant, M. Garreau, S. Nicolai, G. Gryn'ova, C. Corminboeuf, and J. Waser, Chem. Sci. 9, 5883 (2018).
- <sup>85</sup> M. Garreau, F. Le Vaillant, and J. Waser, Angew. Chem. Int. Ed. 58, 8182 (2019).
- 86Y. Liu, X.-L. Chen, X.-Y. Li, S.-S. Zhu, S.-J. Li, Y. Song, L.-B. Qu, and B. Yu, J. Am. Chem. Soc. 143, 964 (2021).
- <sup>87</sup>K. Donabauer, M. Maity, A. L. Berger, G. S. Huff, S. Crespi, and B. König, Chem. Sci. **10**, 5162 (2019).
- <sup>88</sup>Q.-Y. Meng, T. E. Schirmer, A. L. Berger, K. Donabauer, and B. König, J. Am. Chem. Soc. **141**, 11393 (2019).
- 89 K. Matyjaszewski and J. Xia, Chem. Rev. 101, 2921 (2001).
- 90 J. C. Theriot, B. G. McCarthy, C. Lim, and G. M. Miyake, Macromol. Rapid Commun. 38, 1700040 (2017).
- <sup>91</sup>A. Bhattacherjee, M. Sneha, L. Lewis-Borrell, G. Amoruso, T. A. A. Oliver, J. Tyler, I. P. Clark, and A. J. Orr-Ewing, J. Am. Chem. Soc. 143, 3613 (2021).
- <sup>92</sup>M. Sneha, A. Bhattacherjee, L. Lewis-Borrell, I. P. Clark, and A. J. Orr-Ewing, J. Phys. Chem. B 125, 7840 (2021).
- <sup>93</sup>J. C. Theriot, C.-H. Lim, H. Yang, M. D. Ryan, C. B. Musgrave, and G. M. Miyake, Science 352, 1082 (2016).
- <sup>94</sup>M. D. Ryan, J. C. Theriot, C.-H. Lim, H. Yang, A. G. Lockwood, N. G. Garrison, S. R. Lincoln, C. B. Musgrave, and G. M. Miyake, J. Polym. Sci., Part A: Polym. Chem. 55, 3017 (2017).
- 95 J. P. Cole, C. R. Federico, C.-H. Lim, and G. M. Miyake, Macromolecules 52, 747 (2019).
- <sup>96</sup>R. M. Pearson, C.-H. Lim, B. G. McCarthy, C. B. Musgrave, and G. M. Miyake, J. Am. Chem. Soc. 138, 11399 (2016).
- <sup>97</sup>B. McCarthy and G. M. Miyake, ACS Macro Lett. 7, 1016 (2018).
- <sup>98</sup>B. G. McCarthy, R. M. Pearson, C.-H. Lim, S. M. Sartor, N. H. Damrauer, and G. M. Miyake, J. Am. Chem. Soc. **140**, 5088 (2018).
- <sup>99</sup>G. S. Park, J. Back, E. M. Choi, E. Lee, and K. Son, Eur. Polym. J. 117, 347 (2019).
- 100 D. S. Lee, C. S. Kim, N. Iqbal, G. S. Park, K. Son, and E. J. Cho, Org. Lett. 21, 9950 (2019).
- <sup>101</sup>D. Sun, S. V. Rosokha, and J. K. Kochi, J. Am. Chem. Soc. **126**, 1388 (2004).
- 102S. A. Odom, S. Ergun, P. P. Poudel, and S. R. Parkin, Energy Environ. Sci. 7, 760 (2014).
- <sup>103</sup>N. J. Treat, H. Sprafke, J. W. Kramer, P. G. Clark, B. E. Barton, J. Read de Alaniz, B. P. Fors, and C. J. Hawker, J. Am. Chem. Soc. **136**, 16096 (2014).
- 104X. Pan, C. Fang, M. Fantin, N. Malhotra, W. Y. So, L. A. Peteanu, A. A. Isse, A. Gennaro, P. Liu, and K. Matyjaszewski, J. Am. Chem. Soc. 138, 2411 (2016).
- <sup>105</sup>S. Jin, H. T. Dang, G. C. Haug, R. He, V. D. Nguyen, V. T. Nguyen, H. D. Arman, K. S. Schanze, and O. V. Larionov, J. Am. Chem. Soc. **142**, 1603 (2020).
- <sup>106</sup>S. O. Poelma, G. L. Burnett, E. H. Discekici, K. M. Mattson, N. J. Treat, Y. Luo, Z. M. Hudson, S. L. Shankel, P. G. Clark, J. W. Kramer, C. J. Hawker, and J. Read de Alaniz, J. Org. Chem. 81, 7155 (2016).
- 107Y. Zhao, H. Gong, K. Jiang, S. Yan, J. Lin, and M. Chen, Macromolecules 51, 938 (2018).

- <sup>108</sup>K. Jiang, S. Han, M. Ma, L. Zhang, Y. Zhao, and M. Chen, J. Am. Chem. Soc. 142, 7108 (2020).
- 109S. M. Sartor, C. H. Chrisman, R. M. Pearson, G. M. Miyake, and N. H. Damrauer, J. Phys. Chem. A 124, 817 (2020).
- <sup>110</sup>M. Chen, S. Deng, Y. Gu, J. Lin, M. J. MacLeod, and J. A. Johnson, J. Am. Chem. Soc. **139**, 2257 (2017).
- <sup>111</sup> A. M. Martínez-Gualda, R. Cano, L. Marzo, R. Pérez-Ruiz, J. Luis-Barrera, R. Mas-Ballesté, A. Fraile, V. A. de la Peña O'Shea, and J. Alemán, Nat. Commun. 10, 2634 (2019).
- <sup>112</sup>C. Yang, M. D. Kärkäs, G. Magallanes, K. Chan, and C. R. J. Stephenson, Org. Lett. 22, 8082 (2020).
- <sup>113</sup>Y. Zhu, D. Xu, Y. Zhang, Y. Zhou, Y. Yagci, and R. Liu, Angew. Chem. Int. Ed. 60, 16917 (2021).
- <sup>114</sup>A. J. Boyington, C. P. Seath, A. M. Zearfoss, Z. Xu, and N. T. Jui, J. Am. Chem. Soc. 141, 4147 (2019).
- <sup>115</sup>J. Yan, X. Pan, M. Schmitt, Z. Wang, M. R. Bockstaller, and K. Matyjaszewski, ACS Macro Lett. 5, 661 (2016).
- <sup>116</sup>M. Chen, M. J. MacLeod, and J. A. Johnson, ACS Macro Lett. **4**, 566 (2015).
- <sup>117</sup>H. Gong, Y. Zhao, X. Shen, J. Lin, and M. Chen, Angew. Chem. Int. Ed. 57, 333 (2018).
- 118X. Pan, M. Lamson, J. Yan, and K. Matyjaszewski, ACS Macro Lett. 4, 192 (2015).
- <sup>119</sup>K. Kalyanasundaram, Coord. Chem. Rev. **46**, 159 (1982).
- 120 A. Juris, V. Balzani, F. Barigelletti, S. Campagna, P. Belser, and A. V. Zelewsky, Coord. Chem. Rev. 84, 85 (1988).
- <sup>121</sup>M. Gratzel, Acc. Chem. Res. **14**, 376 (1981).
- <sup>122</sup>T. J. Meyer, Acc. Chem. Res. **22**, 163 (1989).
- <sup>123</sup>K. Kalyanasundaram, Coord. Chem. Rev. 177, 347 (1998).
- <sup>124</sup>D. A. Nicewicz and D. W. C. MacMillan, Science **322**, 77 (2008).
- 125 M. A. Ischay, M. E. Anzovino, J. Du, and T. P. Yoon, J. Am. Chem. Soc. 130, 12886 (2008).
- 126 J. M. R. Narayanam, J. W. Tucker, and C. R. J. Stephenson, J. Am. Chem. Soc. 131, 8756 (2009).
- 127 S. Lin, M. A. Ischay, C. G. Fry, and T. P. Yoon, J. Am. Chem. Soc. 133, 19350 (2011)
- 128 M. A. Ischay, M. S. Ament, and T. P. Yoon, Chem. Sci. 3, 2807 (2012).
- 129 M. E. Daub, H. Jung, B. J. Lee, J. Won, M.-H. Baik, and T. P. Yoon, J. Am. Chem. Soc. 141, 9543 (2019).
- 130 J. J. Concepcion, M. K. Brennaman, J. R. Deyton, N. V. Lebedeva, M. D. E. Forbes, J. M. Papanikolas, and T. J. Meyer, J. Am. Chem. Soc. 129, 6968 (2007)
- <sup>131</sup>N. V. Lebedeva, R. D. Schmidt, J. J. Concepcion, M. K. Brennaman, I. N. Stanton, M. J. Therien, T. J. Meyer, and M. D. E. Forbes, J. Phys. Chem. A 115, 3346 (2011).
- 132 C. Bronner and O. S. Wenger, J. Phys. Chem. Lett. 3, 70 (2012).
- 133 M. Kuss-Petermann and O. S. Wenger, J. Phys. Chem. Lett. 4, 2535 (2013).
- <sup>134</sup>R. I. Cukier and D. G. Nocera, Annu. Rev. Phys. Chem. **49**, 337–369 (1998).
- <sup>135</sup>O. S. Wenger, Coord. Chem. Rev. **282–283**, 150 (2015).
- <sup>136</sup>N. Hoffmann, Eur. J. Org. Chem. **2017**, 1982.
- 137 E. C. Gentry and R. R. Knowles, Acc. Chem. Res. 49, 1546 (2016).
- <sup>138</sup>O. S. Wenger, Acc. Chem. Res. 46, 1517 (2013).
- 139 J. D. Nguyen, E. M. D'Amato, J. M. R. Narayanam, and C. R. J. Stephenson, Nat. Chem. 4, 854 (2012).
- 140 E. D. Nacsa and D. W. C. MacMillan, J. Am. Chem. Soc. 140, 3322 (2018).
- <sup>141</sup>X. Guo, Y. Okamoto, M. R. Schreier, T. R. Ward, and O. S. Wenger, Chem. Sci. 9, 5052 (2018).
- <sup>142</sup>C. Kerzig, X. Guo, and O. S. Wenger, J. Am. Chem. Soc. **141**, 2122 (2019).
- 143B. Pfund, D. M. Steffen, M. R. Schreier, M.-S. Bertrams, C. Ye, K. Börjesson, O. S. Wenger, and C. Kerzig, J. Am. Chem. Soc. 142, 10468 (2020).
- 144M. S. Lowry, J. I. Goldsmith, J. D. Slinker, R. Rohl, R. A. Pascal, G. G. Malliaras, and S. Bernhard, Chem. Mater. 17, 5712 (2005).
- 145J. I. Goldsmith, W. R. Hudson, M. S. Lowry, T. H. Anderson, and S. Bernhard, J. Am. Chem. Soc. 127, 7502 (2005).
- <sup>146</sup>I. N. Mills, J. A. Porras, and S. Bernhard, Acc. Chem. Res. **51**, 352 (2018).
- <sup>147</sup>G. J. Choi, Q. Zhu, D. C. Miller, C. J. Gu, and R. R. Knowles, Nature 539, 268 (2016).
- <sup>148</sup>J.-H. Shon and T. S. Teets, Inorg. Chem. **56**, 15295 (2017).

- 149 J.-H. Shon, D. Kim, M. D. Rathnayake, S. Sittel, J. Weaver, and T. S. Teets, Chem. Sci. 12, 4069 (2021).
- 150 J.-H. Shon, D. Kim, T. G. Gray, and T. S. Teets, Inorg. Chem. Front. 8, 3253 (2021).
- <sup>151</sup>R. Bevernaegie, S. A. M. Wehlin, E. J. Piechota, M. Abraham, C. Philouze, G. J. Meyer, B. Elias, and L. Troian-Gautier, J. Am. Chem. Soc. 142, 2732 (2020).
- 152 Y. Wang, X. Zhao, Y. Zhao, T. Yang, X. Liu, J. Xie, G. Li, D. Zhu, H. Tan, and Z. Su, Dyes Pigm. 170, 107547 (2019).
- 153 J.-J. Zhong, W.-P. To, Y. Liu, W. Lu, and C.-M. Che, Chem. Sci. 10, 4883 (2019).
- <sup>154</sup>W. Yang and J. Zhao, Eur. J. Inorg. Chem. **2016**, 5283.
- 155 J.-J. Zhong, Q.-Y. Meng, G.-X. Wang, Q. Liu, B. Chen, K. Feng, C.-H. Tung, and L.-Z. Wu, Chem. Eur. J. 19, 6443 (2013).
- 156 J.-J. Zhong, C. Yang, X.-Y. Chang, C. Zou, W. Lu, and C.-M. Che, Chem. Commun. 53, 8948 (2017).
- <sup>157</sup>H. Na, A. Maity, and T. S. Teets, Organometallics 35, 2267 (2016).
- <sup>158</sup>E. Kabir, D. Patel, K. Clark, and T. S. Teets, Inorg. Chem. 57, 10906 (2018).
- 159 Y. Wu, Z. Wen, J. I. Wu, and T. S. Teets, Chem. Eur. J. 26, 16028 (2020).
- <sup>160</sup>K. Li, X. Guan, C.-W. Ma, W. Lu, Y. Chen, and C.-M. Che, Chem. Commun. 47, 9075 (2011).
- <sup>161</sup>K. Li, G. Cheng, C. Ma, X. Guan, W.-M. Kwok, Y. Chen, W. Lu, and C.-M. Che, Chem. Sci. 4, 2630 (2013).
- <sup>162</sup>K. Li, G. S. Ming Tong, Q. Wan, G. Cheng, W.-Y. Tong, W.-H. Ang, W.-L. Kwong, and C.-M. Che, Chem. Sci. 7, 1653 (2016).
- <sup>163</sup>K. Li, Q. Wan, C. Yang, X.-Y. Chang, K.-H. Low, and C.-M. Che, Angew. Chem. Int. Ed. 57, 14129 (2018).
- 164W. J. Choi, S. Choi, K. Ohkubo, S. Fukuzumi, E. J. Cho, and Y. You, Chem. Sci. 6, 1454 (2015).
- <sup>165</sup>S. B. Harkins and J. C. Peters, J. Am. Chem. Soc. **127**, 2030 (2005).
- <sup>166</sup>S. B. Harkins and J. C. Peters, J. Am. Chem. Soc. 126, 2885 (2004).
- <sup>167</sup>C. Minozzi, A. Caron, J.-C. Grenier-Petel, J. Santandrea, and S. K. Collins, Angew. Chem. Int. Ed. 57, 5477 (2018).
- <sup>168</sup> W. Sattler, M. E. Ener, J. D. Blakemore, A. A. Rachford, P. J. LaBeaume, J. W. Thackeray, J. F. Cameron, J. R. Winkler, and H. B. Gray, J. Am. Chem. Soc. 135, 10614 (2013).
- <sup>169</sup>W. Sattler, L. M. Henling, J. R. Winkler, and H. B. Gray, J. Am. Chem. Soc. 137, 1198 (2015).
- 170 J. Fajardo, J. Schwan, W. W. Kramer, M. K. Takase, J. R. Winkler, and H. B. Grav, Inorg. Chem. 60, 3481 (2021).
- <sup>171</sup>L. A. Büldt, X. Guo, A. Prescimone, and O. S. Wenger, Angew. Chem. Int. Ed. 55, 11247 (2016).
- 172 L. A. Büldt, X. Guo, R. Vogel, A. Prescimone, and O. S. Wenger, J. Am. Chem. Soc. 139, 985 (2017).
- 173P. Herr, F. Glaser, L. A. Büldt, C. B. Larsen, and O. S. Wenger, J. Am. Chem. Soc. 141, 14394 (2019).
- 174H. Yin, P. J. Carroll, J. M. Anna, and E. J. Schelter, J. Am. Chem. Soc. 137, 9234 (2015).
- 175H. Yin, P. J. Carroll, B. C. Manor, J. M. Anna, and E. J. Schelter, J. Am. Chem. Soc. 138, 5984 (2016).
- 176 Y. Qiao, T. Cheisson, B. C. Manor, P. J. Carroll, and E. J. Schelter, Chem.
- Commun. 55, 4067 (2019).

  177 H. Yin, Y. Jin, J. E. Hertzog, K. C. Mullane, P. J. Carroll, B. C. Manor, J. M.
- Anna, and E. J. Schelter, J. Am. Chem. Soc. 138, 16266 (2016). 178Y. Qiao, Q. Yang, and E. J. Schelter, Angew. Chem. Int. Ed. 57, 10999 (2018).
- 179C. D. McTiernan, M. Morin, T. McCallum, J. C. Scaiano, and L. Barriault, Catal. Sci. Technol. 6, 201 (2016).
- <sup>180</sup>D. Stufkens, Coord. Chem. Rev. 177, 127 (1998).
- <sup>181</sup>J. C. Luong, L. Nadjo, and M. S. Wrighton, J. Am. Chem. Soc. **100**, 5790 (1978).
- <sup>182</sup>W. B. Connick, A. J. Di Bilio, M. G. Hill, J. R. Winkler, and H. B. Gray, Inorg. Chim. Acta 240, 169 (1995).
- <sup>183</sup>C. Shih, A. K. Museth, M. Abrahamsson, A. M. Blanco-Rodriguez, A. J. Di Bilio, J. Sudhamsu, B. R. Crane, K. L. Ronayne, M. Towrie, A. Vlček, J. H. Richards, J. R. Winkler, and H. B. Gray, Science 320, 1760 (2008).
- <sup>184</sup>S. Y. Reece and D. G. Nocera, J. Am. Chem. Soc. **127**, 9448 (2005).
- 185 M. Kuss-Petermann, H. Wolf, D. Stalke, and O. S. Wenger, J. Am. Chem. Soc. 134, 12844 (2012).

- <sup>186</sup>A. A. Pizano, J. L. Yang, and D. G. Nocera, Chem. Sci. 3, 2457 (2012).
- 187 F. Glaser, C. Kerzig, and O. S. Wenger, Angew. Chem. Int. Ed. 59, 10266 (2020).
- 188 M. Goez, M. Schiewek, and M. H. O. Musa, Angew. Chem. Int. Ed. 41, 1535 (2002).
- 189 M. Goez, D. von Ramin-Marro, M. H. Othman Musa, and M. Schiewek, J. Phys. Chem. A 108, 1090 (2004).
- <sup>190</sup>I. Ghosh, T. Ghosh, J. I. Bardagi, and B. König, Science **346**, 725 (2014).
- <sup>191</sup>L. Zeng, T. Liu, C. He, D. Shi, F. Zhang, and C. Duan, J. Am. Chem. Soc. 138, 3958 (2016).
- 192 J. He, J. Li, Q. Han, C. Si, G. Niu, M. Li, J. Wang, and J. Niu, ACS Appl. Mater. Interfaces 12, 2199 (2020).
- <sup>193</sup>J. He, Q. Han, J. Li, Z. Shi, X. Shi, and J. Niu, J. Catal. 376, 161 (2019).
- <sup>194</sup>I. Ghosh and B. König, Angew. Chem. Int. Ed. **55**, 7676 (2016).
- 195A. U. Meyer, T. Slanina, A. Heckel, and B. König, Chem. Eur. J. 23, 7900 (2017).
- 196 J. Haimerl, I. Ghosh, B. König, J. Vogelsang, and J. M. Lupton, Chem. Sci. 10, 681 (2019).
- 197 J. I. Bardagi, I. Ghosh, M. Schmalzbauer, T. Ghosh, and B. König, Eur. J. Org. Chem. 2018, 34.
- <sup>198</sup>M. Neumeier, D. Sampedro, M. Májek, V. A. de la Peña O'Shea, A. Jacobi von Wangelin, and R. Pérez-Ruiz, Chem. Eur. J. 24, 105 (2018).
- 199 J. C. Herrera-Luna, D. D. Díaz, M. C. Jiménez, and R. Pérez-Ruiz, ACS Appl. Mater. Interfaces 13, 48784 (2021).
- <sup>200</sup>I. A. MacKenzie, L. Wang, N. P. R. Onuska, O. F. Williams, K. Begam, A. M. Moran, B. D. Dunietz, and D. A. Nicewicz, Nature 580, 76 (2020).
- 201 M. Giedyk, R. Narobe, S. Weiß, D. Touraud, W. Kunz, and B. König, Nat. Catal. 3, 40 (2020).
- <sup>202</sup>T. U. Connell, C. L. Fraser, M. L. Czyz, Z. M. Smith, D. J. Hayne, E. H. Doeven, J. Agugiaro, D. J. D. Wilson, J. L. Adcock, A. D. Scully, D. E. Gómez, N. W. Barnett, A. Polyzos, and P. S. Francis, J. Am. Chem. Soc. 141, 17646 (2019).
- 203 M. L. Czyz, M. S. Taylor, T. H. Horngren, and A. Polyzos, ACS Catal. 11, 5472 (2021).
- 204 M. Goez and D. von Ramin-Marro, Chem. Phys. Lett. 447, 352 (2007).
- 205M. Goez, C. Kerzig, and R. Naumann, Angew. Chem. Int. Ed. 53, 9914 (2014).
- 206C. Kerzig and M. Goez, Chem. Sci. 7, 3862 (2016).
- <sup>207</sup>R. Naumann, C. Kerzig, and M. Goez, Chem. Sci. 8, 7510 (2017).
- <sup>208</sup>R. Naumann, F. Lehmann, and M. Goez, Angew. Chem. Int. Ed. 57, 1078 (2018).
- <sup>209</sup>R. Naumann, F. Lehmann, and M. Goez, Chem. Eur. J. **24**, 13259 (2018).
- <sup>210</sup>R. Naumann and M. Goez, Chem. Eur. J. 24, 9833 (2018).
- <sup>211</sup>R. Naumann and M. Goez, Chem. Eur. J. **24**, 17557 (2018).
- <sup>212</sup>R. Naumann and M. Goez, Green Chem. 21, 4470 (2019).
- <sup>213</sup>Q. G. Mulazzani, S. Emmi, P. G. Fuochi, M. Z. Hoffman, and M. Venturi, J. Am. Chem. Soc. **100**, 981 (1978).
- 214D. Cambié, C. Bottecchia, N. J. W. Straathof, V. Hessel, and T. Noël, Chem. Rev. 116, 10276 (2016).
- 215J. A. Dantas, J. T. M. Correia, M. W. Paixão, and A. G. Corrêa, ChemPhotoChem 3, 506 (2019).
- <sup>216</sup>R. I. Patel, S. Sharma, and A. Sharma, Org. Chem. Front. **8**, 3166 (2021).
- <sup>217</sup>Q. Zhou, Y. Zou, L. Lu, and W. Xiao, Angew. Chem. Int. Ed. 58, 1586 (2019).
- <sup>218</sup>T. H. Rehm, Chem. Eur. J. **26**, 16952 (2020).
- <sup>219</sup>Y. Jiang, K. Xu, and C. Zeng, Chem. Rev. **118**, 4485 (2018).
- 220 H.-T. Tang, J.-S. Jia, and Y.-M. Pan, Org. Biomol. Chem. 18, 5315 (2020).
- 221C. Zhu, N. W. J. Ang, T. H. Meyer, Y. Qiu, and L. Ackermann, ACS Cent. Sci. 7, 415 (2021).
- <sup>222</sup>T. H. Meyer, I. Choi, C. Tian, and L. Ackermann, Chem **6**, 2484 (2020).
- 223S. Möhle, M. Zirbes, E. Rodrigo, T. Gieshoff, A. Wiebe, and S. R. Waldvogel, Angew. Chem. Int. Ed. 57, 6018 (2018).
- 224 A. Matsunaga and A. Yasuhara, Chemosphere 58, 897 (2005).
- 225S. Soualmi, M. Dieng, A. Ourari, D. Gningue-Sall, and V. Jouikov, Electrochim. Acta 158, 457 (2015).
- <sup>226</sup>B. Chen, L.-Z. Wu, and C.-H. Tung, Acc. Chem. Res. 51, 2512 (2018).
- 227Y. Zhong, Y. Wu, B. Chang, Z. Ai, K. Zhang, Y. Shao, L. Zhang, and X. Hao, J. Mater. Chem. A 7, 14638 (2019).

- <sup>228</sup>J.-C. Moutet and G. Reverdy, Tetrahedron Lett. 20, 2389 (1979).
- <sup>229</sup>S. S. Shukla and J. F. Rusling, J. Phys. Chem. **89**, 3353 (1985).
- <sup>230</sup>J. P. Barham and B. König, Angew. Chem. Int. Ed. **59**, 11732 (2020).
- <sup>231</sup>J. Liu, L. Lu, D. Wood, and S. Lin, ACS Cent. Sci. 6, 1317 (2020).
- <sup>232</sup>J. W. Verhoeven, Pure Appl. Chem. **68**, 2223 (1996).
- 233 J. Yang, D. Wang, H. Han, and C. Li, Acc. Chem. Res. 46, 1900 (2013).
- <sup>234</sup>H. G. Cha and K.-S. Choi, Nat. Chem. 7, 328 (2015).
- <sup>235</sup>C. Ding, J. Shi, Z. Wang, and C. Li, ACS Catal. 7, 675 (2017).
- <sup>236</sup>G. G. Bessegato, T. T. Guaraldo, J. F. de Brito, M. F. Brugnera, and M. V. B. Zanoni, Electrocatalysis 6, 415 (2015).
- 237 A. García, C. Fernandez-Blanco, J. R. Herance, J. Albero, and H. García, J. Mater. Chem. A 5, 16522 (2017).
- <sup>238</sup>D. Liu, J.-C. Liu, W. Cai, J. Ma, H. B. Yang, H. Xiao, J. Li, Y. Xiong, Y. Huang, and B. Liu, Nat. Commun. 10, 1779 (2019).
- <sup>239</sup>C. A. Mesa, A. Kafizas, L. Francàs, S. R. Pendlebury, E. Pastor, Y. Ma, F. L. Formal, M. T. Mayer, M. Grätzel, and J. R. Durrant, J. Am. Chem. Soc. 139, 11537 (2017).
- <sup>240</sup>R. Scheffold and R. Orlinski, J. Am. Chem. Soc. **105**, 7200 (1983).
- <sup>241</sup>F. Wang and S. S. Stahl, Angew. Chem. Int. Ed. **58**, 6385 (2019).
- <sup>242</sup>L. Niu, C. Jiang, Y. Liang, D. Liu, F. Bu, R. Shi, H. Chen, A. D. Chowdhury, and A. Lei, J. Am. Chem. Soc. 142, 17693 (2020).
- <sup>243</sup>H. Huang and T. H. Lambert, Angew. Chem. Int. Ed. **59**, 658 (2020).
- <sup>244</sup>H. Huang and T. H. Lambert, Angew. Chem. Int. Ed. **60**, 11163 (2021).
- <sup>245</sup>H. Yan, Z.-W. Hou, and H.-C. Xu, Angew. Chem. Int. Ed. **58**, 4592 (2019).
- <sup>246</sup>X. Lai, X. Shu, J. Song, and H. Xu, Angew. Chem. Int. Ed. **59**, 10626 (2020).

- <sup>247</sup>T. Shen and T. H. Lambert, J. Am. Chem. Soc. 143, 8597 (2021).
- <sup>248</sup>H. Huang, Z. M. Strater, M. Rauch, J. Shee, T. J. Sisto, C. Nuckolls, and T. H. Lambert, Angew. Chem. Int. Ed. 58, 13318 (2019).
- <sup>249</sup>H. Huang, Z. M. Strater, and T. H. Lambert, J. Am. Chem. Soc. **142**, 1698 (2020).
- <sup>250</sup>H. Kim, H. Kim, T. H. Lambert, and S. Lin, J. Am. Chem. Soc. **142**, 2087 (2020).
- <sup>251</sup>H. Huang and T. H. Lambert, J. Am. Chem. Soc. **143**, 7247 (2021).
- 252 T. Shen and T. H. Lambert, Science 371, 620 (2021).
- <sup>253</sup>W. Zhang, K. L. Carpenter, and S. Lin, Angew. Chem. Int. Ed. 59, 409 (2020).
- 254Y. Qiu, A. Scheremetjew, L. H. Finger, and L. Ackermann, Chem. Eur. J. 26, 3241 (2020).
- 255N. G. W. Cowper, C. P. Chernowsky, O. P. Williams, and Z. K. Wickens, J. Am. Chem. Soc. 142, 2093 (2020).
- <sup>256</sup>D. Gosztola, M. P. Niemczyk, W. Svec, A. S. Lukas, and M. R. Wasielewski, J. Phys. Chem. A **104**, 6545 (2000).
- 257M. Marchini, A. Gualandi, L. Mengozzi, P. Franchi, M. Lucarini, P. G. Cozzi, V. Balzani, and P. Ceroni, Phys. Chem. Chem. Phys. 20, 8071 (2018).
- 258C. J. Zeman, S. Kim, F. Zhang, and K. S. Schanze, J. Am. Chem. Soc. 142, 2204 (2020).
- 259 J. S. Beckwith, A. Aster, and E. Vauthey, Phys. Chem. Chem. Phys. 24, 568 (2022).
- 260 A. J. Rieth, M. I. Gonzalez, B. Kudisch, M. Nava, and D. G. Nocera, J. Am. Chem. Soc. 143, 14352 (2021).
- <sup>261</sup>H. Li and O. S. Wenger, Angew. Chem. Int. Ed. **61**, e202110491 (2022).